

# Continental outflow from the US to the upper troposphere over the North Atlantic during the NASA INTEX-NA Airborne Campaign

S. Y. Kim<sup>1</sup>, R. Talbot<sup>1</sup>, H. Mao<sup>1</sup>, D. Blake<sup>2</sup>, S. Vay<sup>3</sup>, and H. Fuelberg<sup>4</sup>

<sup>1</sup>Climate Change Research Center, Institute for the Study of Earth, Oceans, and Space, University of New Hampshire, Durham, NH 03824, USA

<sup>2</sup>Department of Chemistry, University of California – Irvine, Irvine, CA 92697, USA

<sup>3</sup>Chemistry and Dynamics Branch, NASA Langley Research Center, Hampton, VA 23681, USA

<sup>4</sup>Department of Meteorology, Florida State University, Tallahassee, FL 32306, USA

Received: 19 October 2007 – Published in Atmos. Chem. Phys. Discuss.: 28 November 2007

Revised: 20 February 2008 – Accepted: 7 March 2008 – Published: 8 April 2008

**Abstract.** A case of continental outflow from the United States (US) was examined using airborne measurements from NASA DC-8 flight 13 during the Intercontinental Chemical Transport Experiment – North America (INTEX-NA). Mixing ratios of methane (CH<sub>4</sub>) and carbon monoxide (CO) at 8–11 km altitude over the North Atlantic were elevated to 1843 ppbv and 134 ppbv respectively, while those of carbon dioxide (CO<sub>2</sub>) and carbonyl sulfide (COS) were reduced to 372.4 ppmv and 411 pptv respectively. In this region, urban and industrial influences were evidenced by elevated mixing ratios and good linear relationships between urban and industrial tracers compared to North Atlantic background air. Moreover, low mixing ratios and a good correlation between COS and CO<sub>2</sub> showed a fingerprint of terrestrial uptake and minimal dilution during rapid transport over a 1–2 day time period. Analysis of synoptic conditions, backward trajectories, and photochemical aging estimates based on C<sub>3</sub>H<sub>8</sub>/C<sub>2</sub>H<sub>6</sub> strongly suggested that elevated anthropogenic tracers in the upper troposphere of the flight region were the result of transport via convection and warm conveyor belt (WCB) uplifting of boundary layer air over the southeastern US. This mechanism is supported by the similar slope values of linear correlations between long-lived (months) anthropogenic tracers (e.g., C<sub>2</sub>Cl<sub>4</sub> and CHCl<sub>3</sub>) from the flight region and the planetary boundary layer in the southeastern US. In addition, the aircraft measurements suggest that outflow from the US augmented the entire tropospheric column at mid-latitudes over the North Atlantic. Overall, the flight 13 data demonstrate a pervasive impact of US anthropogenic emissions on the troposphere over the North Atlantic.

## 1 Introduction

Continental outflow plays an important role in influencing the chemical environment of the remote troposphere through long-range transport of natural and anthropogenic trace gases and aerosols. Extensive airborne measurements over the Pacific during NASA field campaigns such as PEM-WEST B and TRACE-P have characterized the chemical composition of Asian outflow (Talbot et al., 1997, Blake et al., 2003; Bartlett et al., 2003). Moreover, Asian dust and anthropogenic pollutants via trans-Pacific transport can impact air quality in the US (DeBell et al., 2004; Jaffe et al., 1999, 2003). Recently, long-range transport of Saharan dust over the Pacific route to western North America has been documented in the middle troposphere (McKendry et al., 2007).

One important component of the continental outflow over the north Pacific (Talbot et al., 1996a, 1997) and south Atlantic (Talbot et al., 1996b) basins is wet convective lifting of air masses over the continent with subsequent enhancement in mixing ratios of insoluble trace gases in downwind areas over the ocean at altitudes above 8 km. For example, over the north Pacific Crawford et al. (2003) reported enhanced mixing ratios of CO in the entire 1–11 km vertical column of a cloud impacted area during TRACE-P. A case of deep convective lofting was also obtained during TRACE-A, where a NASA DC-8 flight in the vicinity of a meso-scale complex moving across burning Brazilian savannah measured high levels of biomass combustion products in the middle-to-upper troposphere (Bartlett et al., 1996; Pickering et al., 1996). These scenarios are highly conducive to long-range transport of pollutants due to faster zonal winds aloft and reduced photochemical reactivity.



Correspondence to: S. Y. Kim  
(sk@gust.sr.unh.edu)

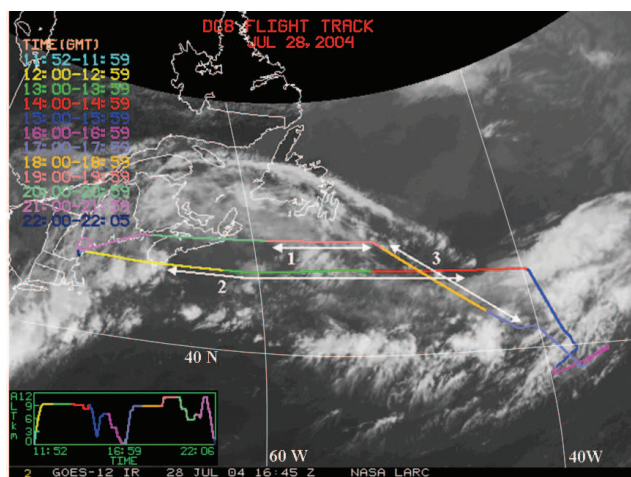


**Fig. 1.** Flight 13 route and the three regions in the upper troposphere.

The International Consortium for Atmospheric Research on Transport and Transformation (ICARTT) field campaign was designed and conducted to gain a better understanding of factors influencing large-scale air quality over North America, the North Atlantic, and western Europe (Fehsenfeld et al., 2006). ICARTT measurement platforms used for studying intercontinental transport included aircraft, ship, satellites, sondes, autonomous balloons, and ground sites that were all operational during July–August 2004. Five types of the North America outflow were classified, which were two types of low level transports, fire plumes, and upper and lower level export by fronts (Methven et al., 2006). Unlike Asian outflow which has been characterized extensively by combustion tracers, a large suite of nonmethane hydrocarbons (NMHCs), and aerosol composition, North America pollutant outflow over the Atlantic has focused largely on ozone ( $O_3$ ) and CO (Dickerson et al., 1995; Mao et al., 2006; Millet et al., 2006; Parrish et al., 1993). North American outflow was characterized comprehensively for its chemical composition during the ICARTT field campaign. Specifically, the large variations in ratios between the pentyl and  $C_2$ – $C_4$  nitrates over the North Atlantic indicated the impact of different parent hydrocarbon emissions from the US to the North Atlantic by photochemical production during transport from the source regions (Reeves et al., 2007). Canadian and Alaskan forest fire emissions caused elevated CO, PAN, organic compounds and aerosols. Moderately high levels of CO and longer-lived hydrocarbons were found in about 44% sampled data which originated from North America by low and upper level outflow (Lewis et al., 2007).

In the northeastern US a primary mechanism for continental outflow is a warm conveyor belt (WCB) transport where a mature cyclone lifts air masses from the boundary layer up into the westerly flow in the upper troposphere (Cooper et al., 2001). The US plumes lofted to the free troposphere by

the WCB can affect air quality in Europe within a few days (Stohl et al., 2003). An extensive field campaign linked elevated trace gas mixing ratios in the lower troposphere over Scandinavia including Alpine areas, to polluted air that was lifted into the free troposphere by the WCB over the eastern US (Huntrieser et al., 2005). A recent modeling study suggested that in summer air masses in the central and southeastern US may be lofted to the free troposphere by convection followed by export to the North Atlantic by the semi-permanent anticyclone (Li et al., 2005). They also pointed out that US regions with the most frequent occurrence of deep convection were the Midwest, the Gulf Coast, and the East Coast. The Gulf Coast and off the East Coast of the US were also found to be influenced by deep convection during a SONEX field campaign over the Atlantic, which was conducted in October–November 1997, by determining lightning activity (Fuelberg et al., 2000).

Here we present a case study of convective uplifting of polluted air to the free troposphere over the southeastern US coupled with rapid transport to the North Atlantic. We utilized data obtained primarily on flight 13 of the NASA DC-8 during the Intercontinental Chemical Transport Experiment – North America (INTEX-NA) component of ICARTT (Singh et al., 2006).

## 2 Methods

### 2.1 Measurement data

INTEX-NA was performed over North America and the adjacent North Atlantic Ocean using the NASA DC-8 aircraft to examine the large-scale distribution of trace gases and aerosols associated with the North America continent (Singh et al., 2006). This study focused on flight 13 which was conducted on 28 July 2004 with one of the main objectives being sampling of US continental outflow as described in Methven et al. (2006) and Arnold et al. (2007). The DC-8 took off at about 12:00 UTC from the Pease International Airport in New Hampshire and landed at around 22:00 UTC, yielding a flight duration of about 10 h. The flight route, shown in Fig. 1, was located over the North Atlantic near the most northerly position of a stationary front and near the southern end of a cold front (Figs. 1 and 2).

A brief description of the overall measurement package on the DC-8 was provided previously in Singh et al. (2006). The principle trace gases of interest here were CO,  $CH_4$ ,  $CO_2$ , COS, and a suite of NMHCs and halocarbons which are archived and available at <http://www-air.larc.nasa.gov/cgi-bin/arcstat>. The majority of the data, including CO and  $CH_4$ , were obtained by the University of California – Irvine (UC-Irvine) (Blake et al., 2003; Colman et al., 2001). Carbon dioxide was measured as described by Vay et al. (1999). Only flight 13 data collected over the Atlantic east of  $70^\circ$  W was used in our analysis. We used



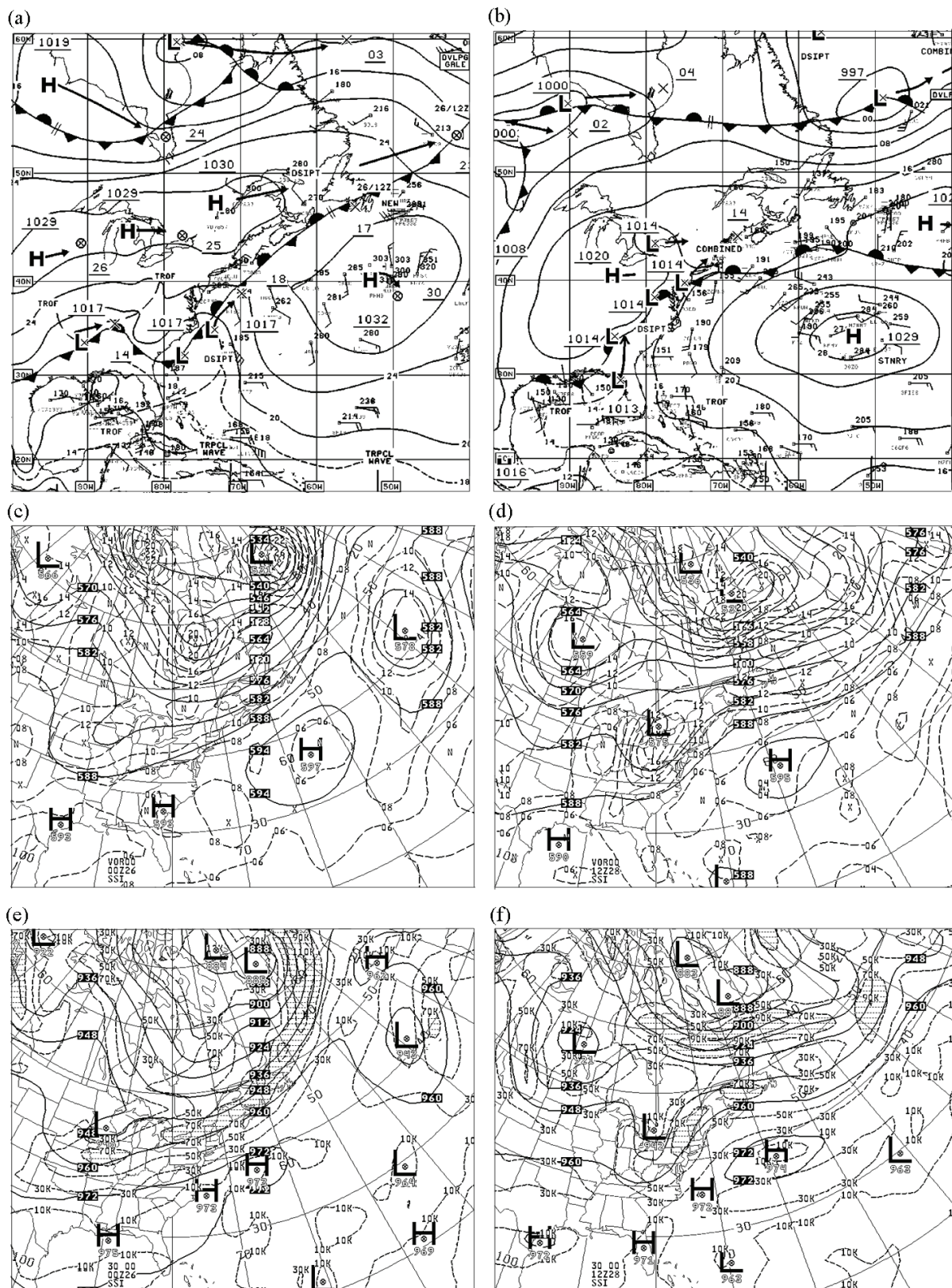


**Fig. 2.** Analyzed sea level pressure (**a and b**) for 12:00 UTC 25 July 2004 and 12:00 UTC 28 July 2004, 500 hPa geopotential height (**c and d**), 300 hPa geopotential height (**e and f**) for 00:00 UTC 26 July 2004 and 12:00 UTC 28 July 2004.

relationships between CH<sub>4</sub>, CO, CO<sub>2</sub>, and COS in boundary layer air (<2 km) over the southeastern US, determined using all the INTEX-NA DC-8 flight data (flights 6, 7, 10, 12, 16, and 19) obtained over the continent at latitudes <35° N, to understand the vertical distribution of trace gases along the flight 13 track. These are all long-lived trace gases, with CO having the shortest lifetime of about 1 to 2 months in summer the range of OH concentration over  $1.0 \times 10^6$ – $1.8 \times 10^6$  molecules cm<sup>-3</sup> (Brasseur et al., 1999; Mak and Southon, 1998). Thus, these trace gases are photochemically stable so that dynamical processes are the most important factors determining their distribution downwind from North America on the transport time scales important to this analysis. NMHCs and halocarbons used in this study were mainly the urban and industrial tracers, C<sub>2</sub>Cl<sub>4</sub>, i-C<sub>5</sub>H<sub>12</sub>, CHCl<sub>3</sub>, and C<sub>6</sub>H<sub>6</sub> (Wang et al., 1995; Chan et al., 2006; Auccott et al., 1999; Na et al., 2001), and a combustion tracer, C<sub>2</sub>H<sub>2</sub>.

We also utilized “Measurement of OZone, water vapor, carbon monoxide and nitrogen oxides by Airbus in-service airCRAFT (MOZAIC)” to examine the vertical distribution of key trace gases over the east coast during the time period of flight 13. MOZAIC uses autonomous instruments loaded into five long-range passenger airliners, namely AIRBUS 340–300 aircraft. Of particular interest here was the four second data obtained on a flight from Vienna, Austria to Washington, D.C. (USA) on 28 July 2004. This dataset provided additional information on the vertical profiles of O<sub>3</sub> and CO over the eastern US between 60° W–78° W and 38° N–48° N obtained during descent into the Washington area.

Ground-level data from the AIRMAP measurement network (<http://airmap.unh.edu>) in the northeastern US for two days in July (27 and 28) 2004 were also utilized in this study. The NMHCs and CO data from Thompson Farm (TF) in Durham, New Hampshire (23 m elevation, 43.11° N and 70.95° W) were 40 min averages and those from the second location on Appledore Island (AI), ME (sea level, 42.97° N and 70.62° W) were 1 hour averages (Sive et al., 2005; Zhou et al., 2005). Methane and CO in ambient air were surveyed for selected US cities by the UC-Irvine group using canisters (Baker et al., 2008). Specifically, we used monthly average values for August collected in the southeastern US cities of Birmingham, Alabama and Baton Rouge, Louisiana during 2001, and Charlotte, North Carolina and Knoxville, Tennessee in 2002, and El Paso, Texas in 2003.

## 2.2 Backward trajectories and photochemical ages

Backward trajectories in combination with an analysis of synoptic conditions and photochemical ages can be an effective method to understand air mass transport. Kinematic backward trajectories were calculated at one minute time steps throughout the INTEX-NA flight series by Florida State University (<http://fuelberg.met.fsu.edu/research/intexa/realtime/>). The ratio of C<sub>3</sub>H<sub>8</sub>/C<sub>2</sub>H<sub>6</sub> was used for comparing

the relative photochemical age of air masses (McKeen and Liu, 1993; Parrish et al., 2004). To assess the relative transport time from the boundary layer in the southeastern US to the flight legs over the North Atlantic, we utilized the chemical clock provided by the reactivity of C<sub>3</sub>H<sub>8</sub> and C<sub>2</sub>H<sub>6</sub> with OH. Equation (1) was used to estimate the transport time:

$$\Delta t = \frac{\ln \frac{(r(\text{C}_3\text{H}_8)/r(\text{C}_2\text{H}_6))_0}{(r(\text{C}_3\text{H}_8)/r(\text{C}_2\text{H}_6))_t}}{(k_{\text{C}_3\text{H}_8} - k_{\text{C}_2\text{H}_6})[\text{OH}]} \quad (1)$$

Here,  $(r(\text{C}_3\text{H}_8)/r(\text{C}_2\text{H}_6))_0$  is the ratio of the mixing ratios of the two compounds in the boundary layer,  $(r(\text{C}_3\text{H}_8)/r(\text{C}_2\text{H}_6))_t$  is the same ratio at a later time  $t$  for each of the flight leg regions of interest,  $k$  is the OH reaction rate constant, and  $[\text{OH}]$  is OH concentration. The DC-8 flight data showed that  $(r(\text{C}_3\text{H}_8)/r(\text{C}_2\text{H}_6))_0$  had a mean value of  $0.36 \pm 0.15$  ( $n=66$ ) for the boundary layer over the southeastern US (hereinafter SBL).

As input for the estimates we used the measured OH mixing ratios, ambient pressures, and air temperatures measured on the DC-8 flights in the SBL. Mean values were 0.18 pptv for OH, 0.92 atm for pressure, and 294 K for temperature, which resulted in a concentration of  $4.1 \times 10^6$  OH molecules cm<sup>-3</sup> in the SBL. We used rate constants for C<sub>3</sub>H<sub>8</sub> and C<sub>2</sub>H<sub>6</sub> of  $1.1 \times 10^{-12}$  cm<sup>3</sup> molecule<sup>-1</sup> s<sup>-1</sup> and  $2.3 \times 10^{-13}$  cm<sup>3</sup> molecule<sup>-1</sup> s<sup>-1</sup> respectively at 294 K (Sander et al., 2003).

## 3 Synoptic meteorology

Shown in Fig. 2a–f are maps of sea level pressure (SLP) for 12:00 UTC on 25 July and 12:00 UTC on 28 July, 500 and 300 hPa geopotential heights for 00:00 UTC on 26 July and 12:00 UTC on 28 July. Together these define the surface, middle and upper tropospheric circulation patterns across the US on the flight day and a few days prior to it. The circulation system that facilitated the transport pattern of Flight 13 evolved from a Canadian Low with cold and warm fronts situated north of Quebec, Canada at 12:00 UTC on 21 July, as shown in the 6 hourly analyzed SLP. This low pressure system was moving eastward with the warm front evolving into an occluded front over the North Atlantic at 12:00 UTC on 23 July, and the cold front remaining largely over the eastern US through 00:00 UTC on 24 July.

The cold front became a stationary front that was located over the eastern US and the western Atlantic starting at 12:00 UTC on 24 July (Fig. 2a and b) and it persisted throughout the duration of flight 13. It should be noted that several small short-lived cyclones were generated in association with the stationary front. In particular, one of these small disturbances was generated over the southeastern US at 06:00 UTC on 26 July and matured into a cyclone which propagated to the Virginia area over the following 24 h. Accompanying the cold front associated with this small cyclone was a WCB over the Southeast. These disturbances and



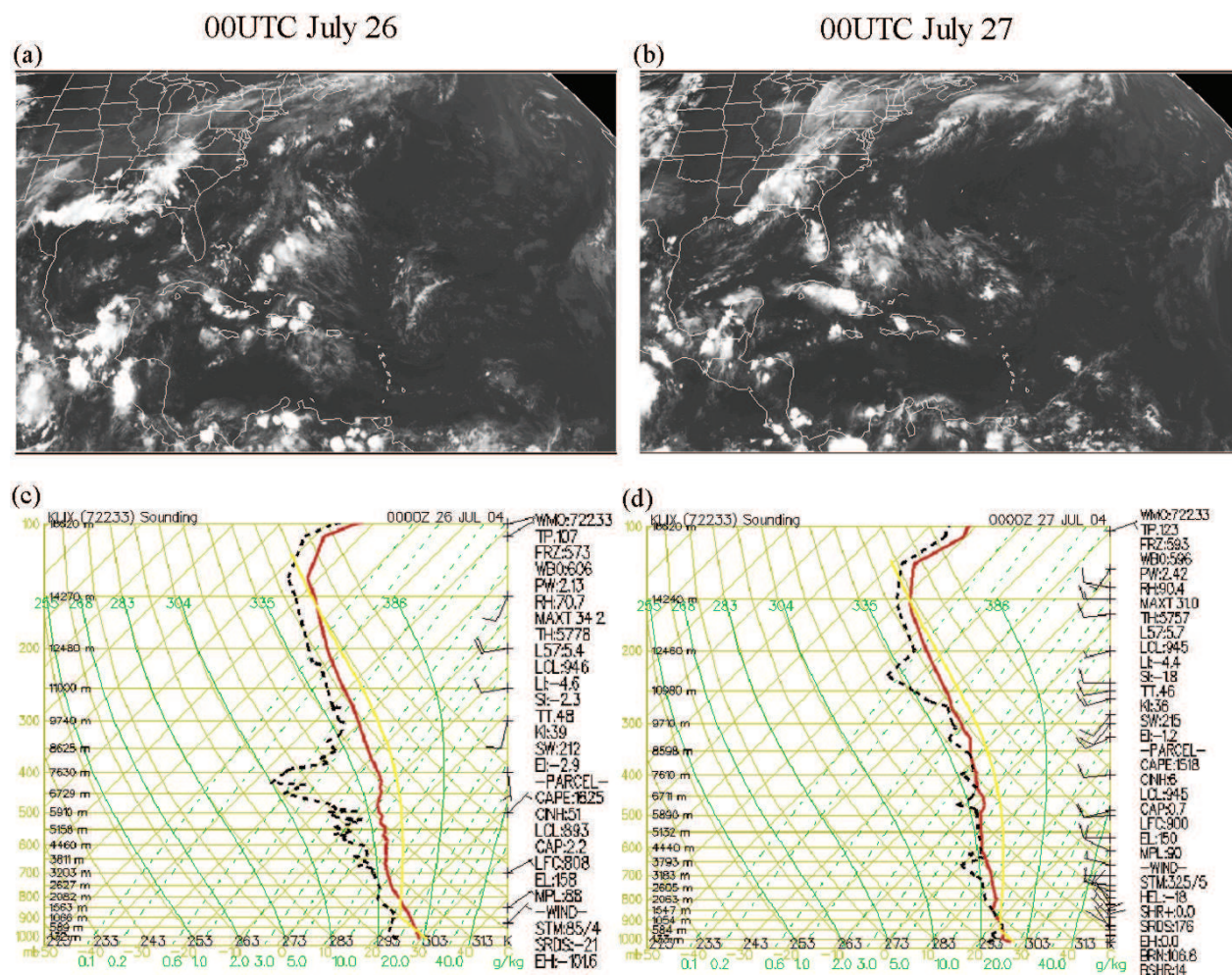


**Fig. 3.** GOES infrared images (a and b), and skew  $T$  and log  $P$  diagram (c and d) at the Slidell, Louisiana (30.33° N and 89.82° W) for 00:00 UTC 26 July 2004 and 00:00 UTC 27 July 2004.

associated WCB are conducive to lifting of boundary layer air masses to the free troposphere.

The 500 hPa geopotential heights at 12:00 UTC on 23 July showed that a trough associated with the Canadian Low was situated over the northern Great Plains. This trough traveled across the Midwest (Fig. 2c) and reached southern Canada in the vicinity of the Great Lakes at 12:00 UTC on 28 July (Fig. 2d). It subsequently moved northeastward relatively fast and weakened over the North Atlantic Ocean. While the influence of this trough existed over the US until 00:00 UTC on 30 July, another trough formed over southern Canada at 12:00 UTC on 28 July (Fig. 2d).

The flow patterns at the 300 hPa geopotential height and isotachs resembled those at the 500 hPa level (Fig. 2e and f). Zonal wind speeds on the 300 hPa level were generally 5–25 m/s over the US, and increased to >35 m/s in the jet stream over the northeastern US. In general, the jet stream on downwind side of trough is associated with upward motion

(Holton, 1992), which facilitates air mass movement from lower altitudes to the upper troposphere with subsequent transport over long distances. Overall, the maps of geopotential height at 500 hPa and 300 hPa together suggested a dynamic westerly flow regime in the mid-to-upper troposphere.

GOES infrared imagery and skew  $T$  and log  $P$  diagrams at 00:00 UTC on 26 and 27 July suggested a strong possibility of upward transport of air masses from the surface during that time period (Fig. 3a–d). GOES infrared imagery (Fig. 3a and b) revealed the presence of high clouds over the eastern US except in coastal regions, extending from Texas eastward to western South Carolina and northeastward to New England. These images indicated cloud top temperatures of 200 K (~14 km altitude), providing the possibility of strong deep convection. Manually digitized radar (MDR) is the best indicator of convection, and Fig. 4a–f showed very large convection occurred over the southeastern and eastern US in the afternoon to the evening for about 3 days between

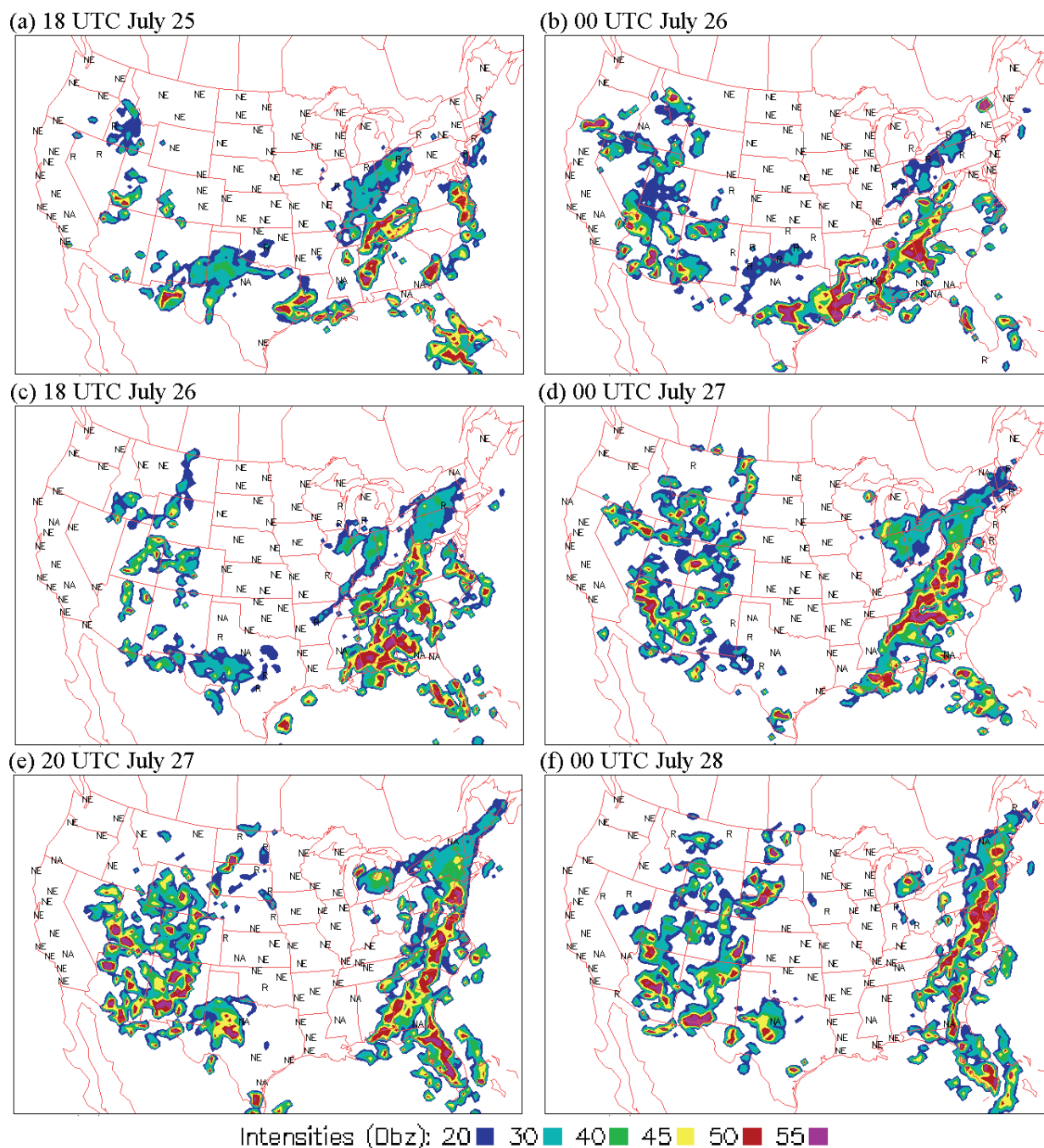


**Fig. 4.** Manually Digitized Radar images for 18:00 UTC and 00UTC 25–28 July 2004. The image of 18:00 UTC 27 July is not available, so 20:00 UTC was in this figure.

25–27 July. Moreover, the area of high clouds coincided with heavy precipitation indicated by the MDR (Figs. 3a–b and 4a–f). Images of other times through 00:00 UTC on 28 July were also examined, and they uniformly suggested similar conditions conducive to convection in this same region.

Furthermore, Skew  $T$  diagrams at individual locations from the eastern US verified the likelihood of convec-

tion. The convective available potential energy (CAPE) and Lifted Index (LI) on the Skew  $T$  diagrams (Fig. 3c and d) from Slidell, Louisiana (30.33° N and 89.82° W), during 25 to 27 July were used to diagnose the presence of local convection. The CAPE values within the range of 1000–2500 J/kg and LI less than  $-4$ , all falling into the criteria for unstable and convective atmospheric conditions



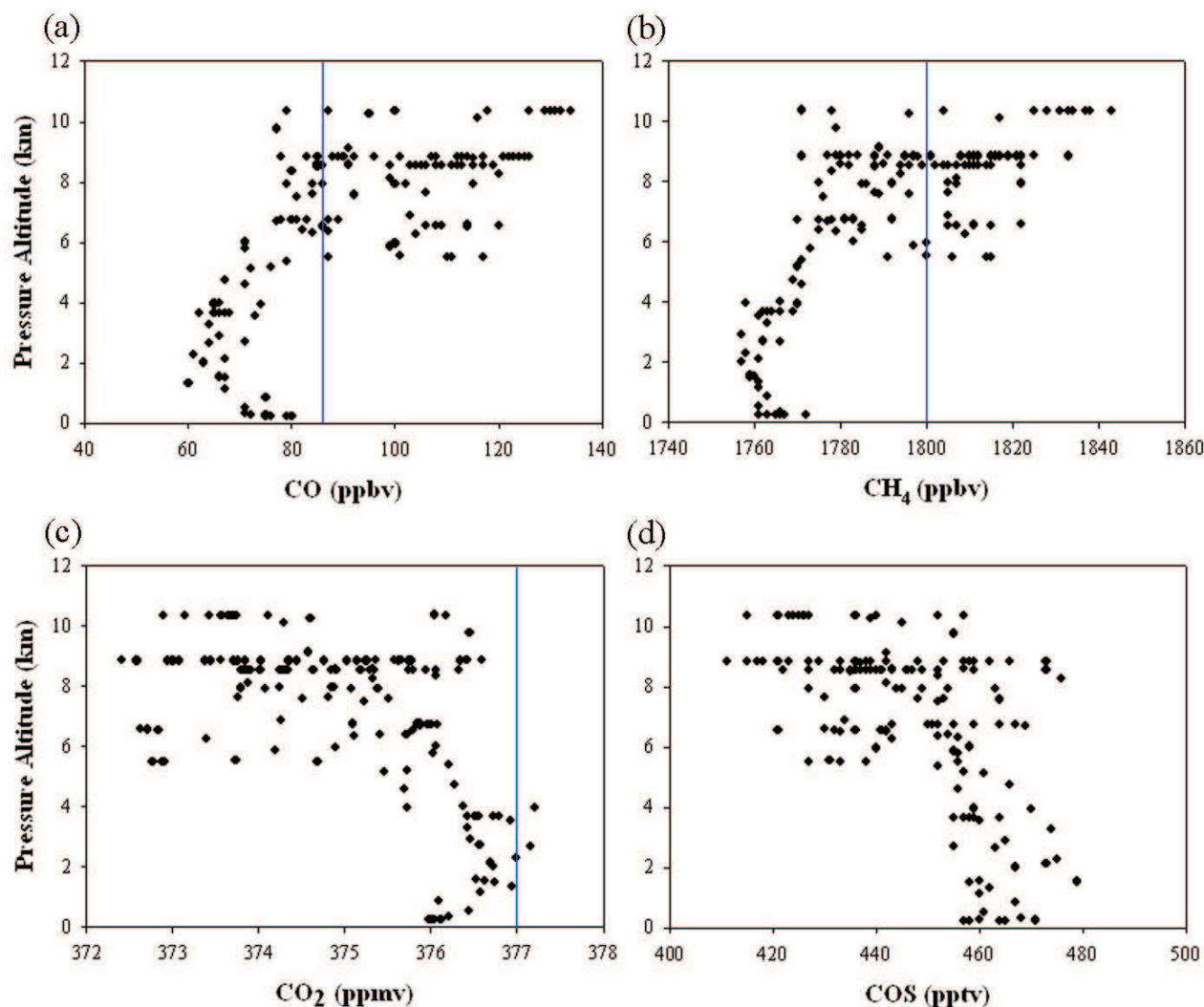


**Fig. 5.** Vertical distribution of (a) CO, (b) CH<sub>4</sub>, (c) CO<sub>2</sub>, and (d) COS. Lines in the graphs are for monthly average mixing ratios in July 2004 in Bermuda.

(<http://www.theweatherprediction.com/severe/indices/>).

In summary, our synoptic analysis suggested that a stationary front associated with a Canadian cyclone over the eastern US continuously induced convection several days before 28 July, which facilitated fast transport of air masses from the boundary layer to the free troposphere. The WCB over the southeastern US also contributed to the vertical transport as indicated by the spawning of small cyclones in association with the stationary front. The mixed effects of widespread convection and the WCB over the southeastern US overlapped in their occurrence during 25–28 July 2004, and were also described in Kiley et al. (2006) and Cooper et al. (2006). All meteorological evidence consistently pointed to combined vertical transport via convection and WCB uplifting combined with fast eastward transport in the free troposphere over the eastern US during the two days prior to flight 13. In the following sections of this paper we exam-

ined the chemical signatures measured at high altitude over the Atlantic to provide support for the meteorological analysis conducted for flight 13.

#### 4 Notable chemical characteristics of flight 13

The vertical distribution of mixing ratios of CO, CH<sub>4</sub>, CO<sub>2</sub>, and COS is displayed for the flight data east of 70° W in Fig. 5. Note that data at altitudes <5 km was obtained near 40° W, not directly underneath of flight legs at altitudes >5 km (Figs. 1 and 5). Mixing ratios of CO near the surface were 70 to 80 ppbv followed by a decrease to the lowest values of ~60 ppbv at 2 km. At altitudes between 2 and 5 km, CO increased to 80 ppbv, and then continued to rise quickly above 5 km varying over a range of 78–134 ppbv at altitudes >8 km. The vertical profile of CH<sub>4</sub> tracked CO

**Table 1.** Chemical characteristics of flight regions and boundary layer in southeastern US.  $\bar{x}(\sigma)$  is mean(standard deviation) and  $q_{0.5}$  means median. The  $n$  is the data number in each region. The units of the compounds are as follows; ppmv for CO<sub>2</sub>, ppbv for CH<sub>4</sub>, CO and O<sub>3</sub>, particles/cm<sup>3</sup> for UCN (ultra fine aerosol), and pptv for the other compounds.

|                                  | Region 1 ( $n=12$ ) |           |             | Region 2 ( $n=28$ ) |           |             | Region 3 ( $n=24$ ) |           |             | Outside ( $n=94$ ) |           |             | Southeastern Boundary ( $n=66$ ) |           |             |
|----------------------------------|---------------------|-----------|-------------|---------------------|-----------|-------------|---------------------|-----------|-------------|--------------------|-----------|-------------|----------------------------------|-----------|-------------|
|                                  | $\bar{x}(\sigma)$   | $q_{0.5}$ | range       | $\bar{x}(\sigma)$   | $q_{0.5}$ | range       | $\bar{x}(\sigma)$   | $q_{0.5}$ | range       | $\bar{x}(\sigma)$  | $q_{0.5}$ | range       | $\bar{x}(\sigma)$                | $q_{0.5}$ | range       |
| CH <sub>4</sub>                  | 1831 (10)           | 1833      | 1804–1843   | 1805 (17)           | 1812      | 1771–1833   | 1808 (8)            | 1810      | 1782–1822   | 1781 (18)          | 1778      | 1757–1822   | 1823 (35)                        | 1820      | 1764–1890   |
| CO                               | 127 (9)             | 130       | 100–134     | 106 (16)            | 113       | 78–126      | 109 (8)             | 110       | 86–119      | 84 (16)            | 80        | 60–120      | 122 (35)                         | 117       | 76–212      |
| CO <sub>2</sub>                  | 373.6 (0.3)         | 373.6     | 372.8–374.2 | 374.5 (1.2)         | 374.4     | 372.4–376.6 | 374.8 (0.8)         | 374.6     | 373.7–376.4 | 375.4 (1.2)        | 375.9     | 372.6–377.3 | 370.2 (6.8)                      | 373.0     | 356.4–379.1 |
| COS                              | 426 (7)             | 425       | 415–440     | 437 (18)            | 433       | 411–473     | 440 (11)            | 438       | 422–473     | 453 (13)           | 456       | 421–479     | 420 (40)                         | 429       | 344–485     |
| O <sub>3</sub>                   | 85 (6)              | 86        | 71–92       | 75 (16)             | 73        | 48–103      | 64 (7)              | 63        | 50–76       | 53 (21)            | 55        | 14–101      | 48 (11)                          | 48        | 27–79       |
| C <sub>2</sub> H <sub>2</sub>    | 117 (16)            | 122       | 79–130      | 93 (28)             | 101       | 38–136      | 94 (14)             | 97        | 55–118      | 45 (29)            | 41        | 11–178      | 140 (96)                         | 120       | 32–428      |
| C <sub>2</sub> Cl <sub>4</sub>   | 10.2 (2.0)          | 10.4      | 5.3–12.4    | 5.1 (1.6)           | 5.5       | 2.6–7.6     | 5.5 (1.1)           | 5.5       | 3.4–6.9     | 3.4 (1.9)          | 2.6       | 1.5–9.3     | 5.8 (4.2)                        | 4.2       | 1.7–19.6    |
| C <sub>2</sub> H <sub>6</sub>    | 928 (96)            | 937       | 659–1089    | 875 (143)           | 892       | 529–1036    | 974 (161)           | 918       | 727–1311    | 571 (228)          | 614       | 258–1031    | 1172 (597)                       | 1013      | 370–3458    |
| i-C <sub>5</sub> H <sub>12</sub> | 9 (3)               | 9         | 3–13        | 12 (5)              | 14        | 4–19        | 12 (4)              | 13        | 3–17        | 7 (3)              | 7         | 3–16        | 109 (84)                         | 93        | 15–506      |
| C <sub>6</sub> H <sub>6</sub>    | 10 (3)              | 11        | 5–13        | 16 (6)              | 18        | 5–24        | 17 (3)              | 17        | 10–22       | 10 (6)             | 9         | 3–43        | 45 (30)                          | 38        | 6–160       |
| CHCl <sub>3</sub>                | 10.5 (0.8)          | 10.7      | 8.9–11.2    | 9.4 (1.0)           | 9.7       | 7.9–10.8    | 9.6 (0.8)           | 9.5       | 8.3–11.4    | 7.8 (1.0)          | 7.5       | 6.2–9.6     | 10.6 (2.9)                       | 10.2      | 6.5–16.8    |
| CF <sub>2</sub> ClBr             | 4.67 (0.12)         | 4.66      | 4.47–4.84   | 4.29 (0.05)         | 4.30      | 4.19–4.36   | 4.32 (0.09)         | 4.32      | 4.18–4.61   | 4.23 (0.11)        | 4.19      | 4.09–4.59   | 4.33 (0.08)                      | 4.33      | 4.13–4.49   |
| UCN                              | 10172 (2436)        | 10833     | 2476–11340  | 1482 (975)          | 1400      | 146–3574    | 1998 (1168)         | 1548      | 720–5517    | 1542 (2348)        | 694       | 129–10427   | 3988 (3852)                      | 2611      | 334–15327   |
| CS <sub>2</sub>                  | 3.2 (3.6)           | 1.5       | 1.1–14.0    | 4.0 (2.5)           | 3.2       | 1.2–11.2    | 2.7 (1.8)           | 2.1       | 1.2–9.3     | 3.2 (2.9)          | 2.4       | 1.1–21.0    | 9.3 (7.9)                        | 6.8       | 1.7–39.2    |

closely, which exhibited levels of 1760 to 1770 ppbv near the surface followed by a slight decrease at 2 km. Between 2 and 5 km CH<sub>4</sub> again hovered around 1770 ppbv. An increasing trend with altitude was accelerated above 5 km, where CH<sub>4</sub> was enhanced up to 1843 ppbv at 8–11 km.

The vertical profiles of CO<sub>2</sub> and COS showed trends opposite those of CO and CH<sub>4</sub>. Mixing ratios of CO<sub>2</sub> were  $\sim 376$  ppmv near the surface, and then increased to 377 ppmv at 2 km followed by a decrease to  $\sim 375.5$  ppmv between 2 and 5 km and further decrease above 5 km. The minimum value of 372.4 ppmv was observed in the 8–11 km region. COS tracked CO<sub>2</sub> closely with mixing ratios varying over 455–475 pptv near the surface, increasing to 480 pptv at 2 km, and then decreasing gradually to 455 pptv between 2 and 5 km. The lowest COS mixing ratios near 410 pptv were found at 8–11 km.

To understand the causes for the high mixing ratios of CO and CH<sub>4</sub> that occurred in the 8–11 km altitude region, we identified three time periods with the most enhanced levels (Fig. 1). These occurred on constant altitude flight legs, with the first region at 10.4 km over the time period of 19:00–20:00 UTC, the second at 8.9 km during 12:20–14:40 UTC, and the third at 8.5 km over 17:30–19:00 UTC. All other segments of the flight are referred to as “Outside” (i.e., outside of the three regions), and they are discussed in Sect. 5.

First, we used trace gas data from the NOAA Global Monitoring Division (GMD) monitoring site on Bermuda (<http://www.esrl.noaa.gov/gmd/dv/ftpdata.html>) and from Mace Head, Ireland (Simmonds et al., 2006) to determine representative background mixing ratios over the North Atlantic. The monthly average surface mixing ratio at Bermuda in July 2004 was 1800 ppbv for CH<sub>4</sub>, 86 ppbv for CO, and 377 ppmv for CO<sub>2</sub>. The mean mixing ratio of C<sub>2</sub>Cl<sub>4</sub> at Mace Head, Ireland was  $4.94 \pm 0.06$  pptv from measurements over the period of 2000 to 2004 (Simmonds et al., 2006). In two rural areas of the US, annual mean surface mixing

ratios of COS from February 2002 to February 2005 were  $444 \pm 8$  pptv in Wisconsin and  $441 \pm 8$  pptv at Harvard Forest, Massachusetts (Montzka et al., 2007).

Statistics are provided in Table 1 to describe the chemical environment of the three regions of enhanced mixing ratios. CO, C<sub>2</sub>H<sub>2</sub> and C<sub>2</sub>Cl<sub>4</sub> exhibited mean mixing ratios of 127 ppbv, 117 pptv and 10.2 pptv, respectively, in region 1, 106 ppbv, 93 pptv and 5.1 pptv in region 2, and 109 ppbv, 94 pptv and 5.5 pptv in region 3. Correspondingly, in regions 1, 2, and 3 the mean value of CH<sub>4</sub> was 1831 ppbv, 1805 ppbv, and 1808 ppbv respectively. Compared to the background levels over the North Atlantic, the mean levels of CH<sub>4</sub>, CO, and C<sub>2</sub>Cl<sub>4</sub> in regions 1, 2, and 3 were higher by 0–1.7%, 23–48%, and 3.3–106% respectively. Mixing ratios of CS<sub>2</sub>, whose primary source is chemical industrial processing (Chin and Davis, 1993), were mainly less than 4 pptv in each region with occasional levels up to 14 pptv. Overall, the three regions showed a clear influence of urban combustion emissions.

The air mass transport time to the free troposphere can be estimated by combining hydrocarbon lifetimes and trajectories whether the transport was by the WCB on the synoptic scale or mesoscale convection (Purvis et al., 2003). This transport was investigated here using backward trajectories combined with photochemical age estimates of air masses in regions 1–3. Kinematic 5-day backward trajectories arriving in each of the three regions are presented in Fig. 6. Since many of the air masses appeared to meander over the southeastern US for several days, 10-day backward trajectories (not shown) were used to examine the long-range transport of these air masses to the US. In the case of region 1, these trajectories showed mainly two origins, with one from over the eastern Pacific/US west coast and the other from the Gulf of the Mexico. These air masses arrived over the southeastern US in the mid-to-upper troposphere, and then spent  $\sim 4$  days over the southeastern US in the altitude region of



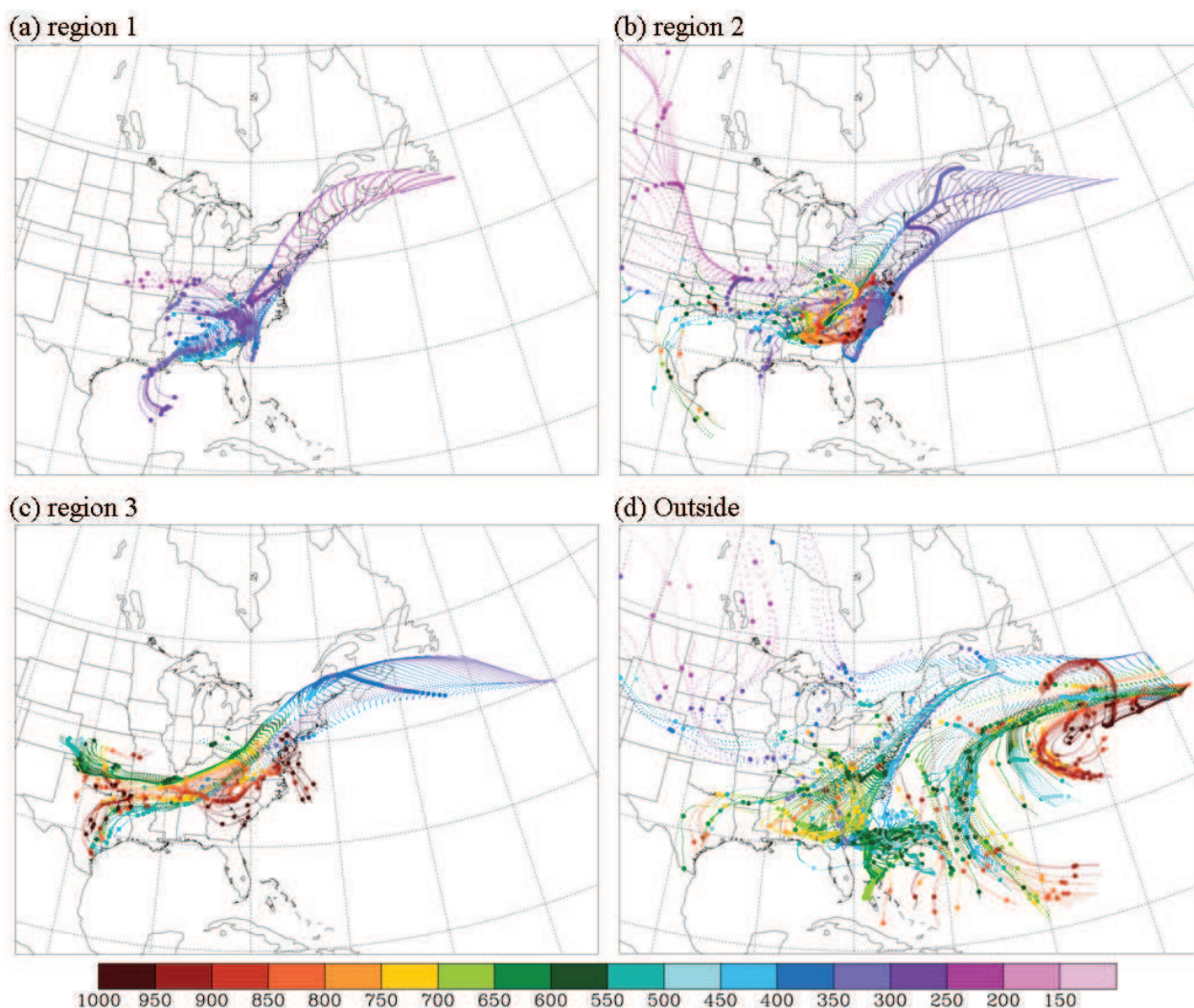


**Fig. 6.** Kinematic 5-day backward trajectories for each region. Big dots are at 00:00 UTC on each day and the small ones are other hours. Unit of color bar is hPa.

550 to 300 hPa. Eventually they were transported in <20 h from over the Virginia area at 00:00 UTC on 28 July to region 1 in the upper troposphere (>350 hPa). The mean value of  $C_3H_8/C_2H_6$  was  $0.23 \pm 0.02$  in region 1, and photochemical aging of an SBL air mass arriving in region 1 was 1.5 days based on Eq. (1).

The backward trajectories for region 2 illustrated a complex dynamical situation. In this case there were a large number of trajectories indicating that the air spent 3–4 days over the southeastern US at altitudes ranging from near the surface to 500 hPa. In addition, approximately 13% of the trajectories followed zonal westerly flow at 300 hPa which intercepted the air masses residing over the southeastern US for several days. Ten-day backward trajectories indicated that the inflowing air had arrived from over the northwestern US, the North Pacific, and the Gulf of the Mexico. On 27 July this mixture of air masses was quickly advected over the North-

east, and arrived at the flight altitude on 28 July. The value of  $C_3H_8/C_2H_6$  was  $0.20 \pm 0.04$  in this region, and the photochemical aging of an SBL air mass arriving in region 2 was 2 days.

Air masses transported to region 3 had their origin over mainly the south central and southeastern US. It appears that boundary layer air over eastern Texas was advected at low level to the southeastern states and mixed with SBL air during vertical lifting on 27 July and mid-tropospheric air masses that originated over the Oklahoma/Colorado area. On the 28th the air passed over the Northeast in the mid-troposphere and arrived at the flight altitude of 8.5 km nearly coincident in time with the region 1 air masses. It appears that it took about 1.7 days to reach the air masses to the flight region 3. The value of  $C_3H_8/C_2H_6$  was  $0.22 \pm 0.03$  in region 3, and photochemical aging of an SBL air mass arriving in this region was 1.7 days.

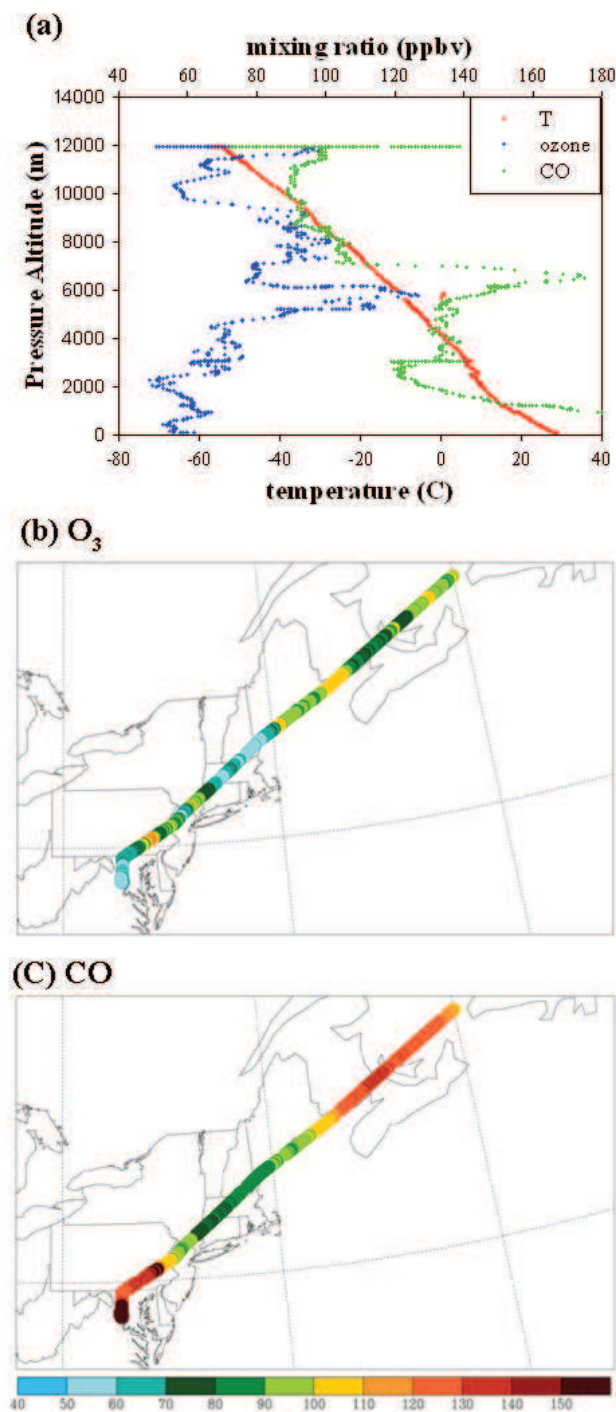


**Fig. 7.** The vertical profiles of temperature, O<sub>3</sub>, and CO (a) obtained from the MOZAIC flights landing in Washington, D.C. on 28 July 2004, and the horizontal distributions of O<sub>3</sub> (b) and CO (c) during the flights. The unit of color bar is ppbv.

We also estimated the chemical clock transport times in these three regions using ratios of ethyne/CO and trichloroethylene/tetrachloroethylene (C<sub>2</sub>HCl<sub>3</sub>/C<sub>2</sub>Cl<sub>4</sub>). In

general, these produced variable transport times that varied by up to a factor of two from C<sub>3</sub>H<sub>8</sub>/C<sub>2</sub>H<sub>6</sub>. Using a lower OH concentration suggested by Arnold et al. (2007) also produced transport times that were about two times longer. We believe that for flight 13 the trajectory estimated transport times are more reliable than those estimated by the chemical clock method. This is likely due to the air masses lingering over the US for several days and entraining multiple inputs of boundary layer air by convection over the SBL. This likely produced a very mixed air mass of various ages and is responsible for the inconsistent chemical clock transport times.

Backward trajectories and the synoptic weather patterns indicated that the SBL air masses were sampled in regions 1–3 due to their fast transport through convection and the WCB that developed in association with the stationary front. Ultrafine aerosol showed distinct mean differences of 10 172 particles/cm<sup>3</sup> in region 1, 1482 particles/cm<sup>3</sup> in region 2, and 1998 particles/cm<sup>3</sup> in region 3. A high degree of correlation between enhanced condensation nuclei number densities and mixing ratios of CO, CH<sub>4</sub>, NO, and OH has been observed in air masses influenced by deep convection over the central US (Twohy et al., 2002). However, we did not find such correlation in the three regions in spite of the very high concentrations of ultrafine aerosols and increased mixing ratios of CO. Wang et al. (2000) observed high concentration of condensation nuclei (>10 000 cm<sup>-3</sup>) in the upper troposphere associated with convection using the NO/NO<sub>y</sub> ratio as a chemical clock. They also pointed out that high CN concentration from aircraft emissions in the upper troposphere was not sampled frequently because of faster dilution than the transport of the boundary layer air aloft via convection. Although our results do not parallel those of Twohy et al. (2002), our analysis implies an impact of convective outflow in region 1 similar to the analysis of Wang et al. (2000). In addition, a diagnostic indicator of wet convection is the ratio of CH<sub>3</sub>OOH/H<sub>2</sub>O<sub>2</sub>, since H<sub>2</sub>O<sub>2</sub> is removed preferentially by wet scavenging compared to CH<sub>3</sub>OOH resulting in ratio values >1 (Talbot et al., 1996b). Snow et al. (2007) found that ratios of <1 for H<sub>2</sub>O<sub>2</sub>/CH<sub>3</sub>OOH and <100 ppbv for O<sub>3</sub> indicated convection during the ICARTT study. The flight 13 measurements showed lower mean values of H<sub>2</sub>O<sub>2</sub>/CH<sub>3</sub>OOH which were 1.3, 2.6, and 2.2 in regions 1–3, respectively, than a value of 3.1 from the SBL. The ratio ranges were 0.77–2.15 for region 1, 0.25–5.34 for region 2, and 1.16–3.72 for region 3, suggesting that convection impacted regions 1 and 2. Overall, our analysis suggests that region 1 was mostly influenced by deep convective vertical transport, whereas regions 2 and 3 appear to be dominated by lofting of air by the WCB.

The photochemical ages estimated from C<sub>3</sub>H<sub>8</sub>/C<sub>2</sub>H<sub>6</sub> in regions 1, 2, and 3 are reasonably similar to the transport times deduced from the backward trajectories which corroborates fast transport with minimal apparent dilution of SBL air by aged background air. Evidence for minimal mixing is provided by similar mixing ratios of CHCl<sub>3</sub> between regions 1–3

(9.4–10.5 pptv) and SBL (10.6 pptv). Additional evidence is the preserved low mixing ratios of CO<sub>2</sub> and COS, which are typical of boundary layer air influenced by biospheric activity during the growing season. The mean mixing ratios of CO<sub>2</sub> in regions 1–3 were between 373.5 and 375 ppmv, and these were lower by 0.6–1% than the background mixing ratio from surface measurements at Bermuda. In comparison, mean mixing ratios of COS in regions 1, 2, and 3 (426–440 pptv) were closer to values found in the SBL over the US. The low mixing ratios of COS found in the upper troposphere during flight 13 is indicative of efficient terrestrial COS uptake in the SBL (Sandoval-Soto et al., 2005).

The backward trajectories suggested that the air masses arriving in the three study regions spent 1–4 days over the southeastern US and were then transported to the Northeast and upward by fast zonal flow in the middle and upper troposphere on 27–28 July. If the transport from the SBL to the flight regions was indeed rapid, then the effect of dilution and in situ chemical processing can be small, and subsequently the mixing ratios of trace gases in the source and flight regions should be similar. Mixing ratios of tracers in the SBL were thus compared with upper tropospheric values (Table 1). In general, industrial or urban tracers in the SBL exhibited higher levels than those in each flight region except for C<sub>2</sub>Cl<sub>4</sub>. This result is reasonable since some dilution would be expected during transport of SBL air to the upper troposphere. Enhanced mixing ratios of other urban tracers (e.g., C<sub>2</sub>Cl<sub>4</sub> and CHCl<sub>3</sub>) and high concentrations of ultrafine aerosol were also observed as evidence of urban impacted air masses in the upper troposphere. In the apparent SBL source region there are significant urban and industrial sources based on the emissions map of CHCl<sub>3</sub> (Aucott et al., 1999). The region is also widely covered with abundant vegetation as evidenced by isoprene emissions (Fiore et al., 2005), which accounts for uptake of COS and CO<sub>2</sub> and consequently their reduced mixing ratios.

MOZAIC measurements were used as an independent source of data on air mass composition over the Atlantic and eastern US. One of the instrumented flights into Washington, D.C. from Europe on 28 July was essentially routed through the region of interest here. MOZAIC data collected at 16:20–19:00 UTC on 28 July sampled the upper troposphere where the rapid transport of SBL air masses seemingly occurred from 00:00 UTC on 27 July to 16:00 UTC on 28 July. The MOZAIC CO and O<sub>3</sub> spatial distributions are shown in Fig. 7. According to the backward trajectories, region 1 of flight 13 and the MOZAIC sampling route overlapped geographically over New Brunswick, Nova Scotia, and the adjacent Oceanic area. The MOZAIC data showed mixing ratios of CO as large as 140 ppbv in the upper troposphere (~12 km). Ozone was between 74 and 110 ppbv for the data in the area with CO > 100 ppbv, and a negative slope of –0.6 was identified for the O<sub>3</sub>–CO correlation. Coincident high levels of CO and O<sub>3</sub> generally indicate polluted air masses, while high O<sub>3</sub> (O<sub>3</sub> > 100 ppbv) alone sug-

gests a weak stratospheric influence. These data together with the flight 13 measurements support a broad influence of US outflow to the upper troposphere over the Atlantic Ocean by the deep trough system. Upon descent into a polluted layer over Washington D.C., CO mixing ratios up to 175 ppbv were identified between 5 and 7 km (39.9–40.5° N, and 75.6–76.6° W). This polluted layer likely originated in the boundary layer over the US but did not get entrained in the flow pathway of the flight 13 upper tropospheric air masses. However, the HYSPLIT backward trajectories were not able to resolve this because of the inadequate vertical resolution.

We explored the possibility of an Asian impact on the flight 13 upper tropospheric study area as found on flights 3, 8, 10, 15 and 20 by Liang et al., (2007). Halon-1211 (CBrClF<sub>2</sub>), an important tracer of Asian polluted outflow (Blake et al., 2003), averaged 4.3 pptv over the flight 13 route, similar to background levels in boundary layer air over the western Pacific during TRACE-P, 4.3±0.04 pptv of CBrClF<sub>2</sub> (Barletta et al., 2006). Our backward trajectories analysis presented earlier and the key tracers indicated that Asian emissions did not affect directly the flight 13 region, and suggests that the outflow from the US dominated the pollution in the study area.

## 5 Outside air mass chemical composition

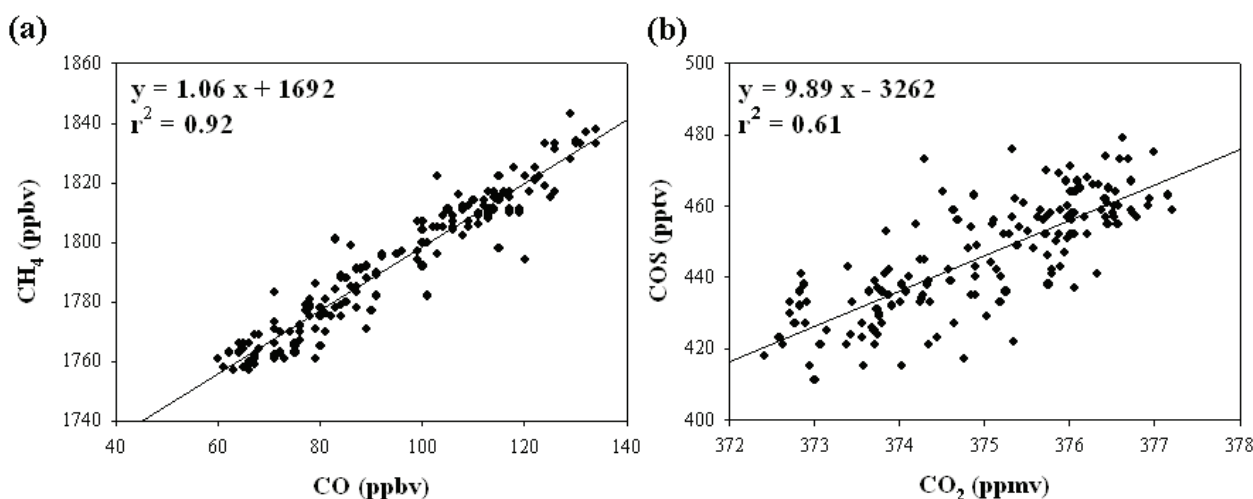
As mentioned in Sect. 4, the Outside air included all segments except measurements from regions 1–3. Hence different altitudes and geographical locations were mixed for the Outside data. The average chemical composition of the Outside air can be summarized to have an average composition of 84 ppbv CO, 375.4 ppmv CO<sub>2</sub>, 1781 ppbv CH<sub>4</sub>, 453 pptv COS, 45 pptv C<sub>2</sub>H<sub>2</sub>, 3.4 pptv C<sub>2</sub>Cl<sub>4</sub>, and 53 ppbv O<sub>3</sub>. To find out whether the Outside chemical composition was similar to the North Atlantic background air, we again compared the airborne measurements with those from the NOAA GMD monitoring site on Bermuda and Mace Head (Simmonds et al., 2006). The results of this comparison showed that CH<sub>4</sub>, CO, C<sub>2</sub>Cl<sub>4</sub> and CO<sub>2</sub> were lower than at Bermuda and Mace Head by 1.1%, 2.4%, 30.6%, and 0.4% respectively. Comparison of the mean values indicated that the Outside air was not affected by fresh urban and industrial source emissions. However, the mixing ratios of trace gases in the Outside air varied over wider ranges than those in regions 1, 2, and 3. In fact, maximum mixing ratios of CS<sub>2</sub>, C<sub>6</sub>H<sub>6</sub>, and C<sub>2</sub>H<sub>2</sub> were even larger than those in the three regions.

Backward trajectories for the Outside region indicated the possibility of air masses with diverse origins (Fig. 6), which were categorized qualitatively into four source regions. The fractional contribution for each source region was estimated by comparison of the number of trajectories from each area to the total for the Outside. It was found that ~44% of air masses in the Outside area were from US outflow, ~28%



**Table 2.** Chemical Characteristics of “Outside” Air of flight 13. Denotations and units are the same as Table 1.

| The outside                      | US outflow ( <i>n</i> =34) |                         |             | The western Atlantic ( <i>n</i> =29) |                         |             | The remote Central Atlantic ( <i>n</i> =26) |                         |             | Pacific ( <i>n</i> =5) |                         |             |
|----------------------------------|----------------------------|-------------------------|-------------|--------------------------------------|-------------------------|-------------|---|-------------------------|-------------|------------------------|-------------------------|-------------|
|                                  | $\bar{x}(\sigma)$          | <i>q</i> <sub>0.5</sub> | range       | $\bar{x}(\sigma)$                    | <i>q</i> <sub>0.5</sub> | range       | $\bar{x}(\sigma)$                           | <i>q</i> <sub>0.5</sub> | range       | $\bar{x}(\sigma)$      | <i>q</i> <sub>0.5</sub> | range       |
| CH <sub>4</sub>                  | 1798 (14)                  | 1799                    | 1771–1822   | 1775 (11)                            | 1775                    | 1757–1805   | 1764 (3)                                    | 1763                    | 1759–1772   | 1789 (12)              | 1792                    | 1775–1805   |
| CO                               | 98 (13)                    | 100                     | 77–120      | 77 (10)                              | 78                      | 61–106      | 69 (5)                                      | 68                      | 60–80       | 98 (15)                | 100                     | 84–120      |
| CO <sub>2</sub>                  | 374.2 (1.1)                | 374.3                   | 372.6–376.5 | 376.0 (0.6)                          | 375.9                   | 373.7–377.3 | 376.4 (0.3)                                 | 376.5                   | 375.9–377.2 | 374.9 (0.4)            | 374.9                   | 374.2–375.4 |
| COS                              | 442 (10)                   | 442                     | 421–464     | 457 (9)                              | 457                     | 430–475     | 463 (6)                                     | 461                     | 455–479     | 459 (12)               | 457                     | 445–476     |
| O <sub>3</sub>                   | 70 (10)                    | 71                      | 44–92       | 54 (15)                              | 55                      | 23–83       | 28 (12)                                     | 25                      | 14–47       | 63 (23)                | 57                      | 43–101      |
| C <sub>2</sub> H <sub>2</sub>    | 68 (18)                    | 70                      | 40–102      | 37 (15)                              | 35                      | 14–84       | 18 (3)                                      | 17                      | 11–26       | 87 (55)                | 79                      | 41–178      |
| C <sub>2</sub> Cl <sub>4</sub>   | 5.4 (1.7)                  | 5.2                     | 2.6–9.3     | 2.4 (0.5)                            | 2.4                     | 1.6–4.3     | 1.8 (0.1)                                   | 1.7                     | 1.5–2.2     | 3.9 (0.7)              | 4.1                     | 2.9–4.5     |
| C <sub>2</sub> H <sub>6</sub>    | 757 (112)                  | 758                     | 606–1002    | 561 (205)                            | 577                     | 258–1031    | 306 (24)                                    | 303                     | 260–343     | 739 (142)              | 769                     | 596–934     |
| i-C <sub>5</sub> H <sub>12</sub> | 8 (4)                      | 8                       | 3–16        | 6 (4)                                | 6                       | 3–8         | NA  | NA                      | NA          | 7 (2)                  | 6                       | 5–9         |
| C <sub>6</sub> H <sub>6</sub>    | 12 (5)                     | 11                      | 3–23        | 7 (3)                                | 6                       | 3–12        | NA  | NA                      | NA          | 18 (15)                | 16                      | 6–43        |
| CHCl <sub>3</sub>                | 8.7 (0.7)                  | 8.9                     | 7.3–9.6     | 7.3 (0.6)                            | 7.3                     | 6.3–9.3     | 7.0 (0.4)                                   | 7.1                     | 6.2–7.6     | 8.8 (0.8)              | 9.1                     | 7.7–9.6     |
| CF <sub>2</sub> ClBr             | 4.37 (0.1)                 | 4.36                    | 4.18–4.59   | 4.19 (0.06)                          | 4.19                    | 4.11–4.31   | 4.15 (0.03)                                 | 4.15                    | 4.09–4.23   | 4.24 (0.05)            | 4.24                    | 4.20–4.29   |
| UCN                              | 3390 (3387)                | 1840                    | 355–10427   | 885 (557)                            | 766                     | 357–2666    | 328 (78)                                    | 340                     | 180–447     | 343 (317)              | 218                     | 129–809     |

**Fig. 8.** Correlations (a) between CO and CH<sub>4</sub>, and (b) between CO<sub>2</sub> and COS on flight 13.

originated from the western Atlantic, ~20% from the remote Central Atlantic, and ~8% from over the North Pacific.

Chemical environments corresponding to the four source regions were summarized in Table 2. The average mixing ratio of CO, C<sub>2</sub>H<sub>2</sub> and C<sub>2</sub>Cl<sub>4</sub> were highest at 98 ppbv, 68 pptv and 5.4 pptv respectively in US outflow, and lowest at 69 ppbv, 18 pptv and 1.8 pptv in air from the remote Central Atlantic. The average levels of O<sub>3</sub>, CH<sub>4</sub>, selected anthropogenic NMHCs, and ultrafine aerosol followed the same source distribution. For example, the average mixing ratio of O<sub>3</sub> showed the highest level of 70 ppbv in the US outflow, and the lowest of 28 ppbv in air masses from the remote Central Atlantic. However, CO<sub>2</sub> and COS exhibited opposite variation, with higher mixing ratios from source regions far away from the North American continent. Specifically, the average mixing ratios of CO<sub>2</sub> and COS were 374.2 ppmv and 442 pptv respectively in the US outflow, 376.0 ppmv and 457 pptv in air from the western Atlantic, 376.4 ppmv and 463 pptv from over the remote Cen-

tral Atlantic, and 374.9 ppmv and 459 pptv from the Pacific. These results clearly show the role of the terrestrial biosphere in modulating CO<sub>2</sub> and COS in the troposphere downwind of a continental area.

## 6 Chemical characterization using correlation analysis

The slope of the standard linear regression between correlated chemical compounds can be a useful source identifier (Xiao et al., 2004). Based on the similar vertical distributions recognizable from Fig. 5, correlation of the pairs CH<sub>4</sub>-CO and COS-CO<sub>2</sub> was examined using all data from flight 13 (Fig. 8). Carbon monoxide and CH<sub>4</sub> were correlated remarkably well at  $r^2=0.92$ . This implies that anthropogenic sources had a major impact on CH<sub>4</sub> mixing ratios at all altitudes sampled on flight 13 over the North Atlantic. The correlation between COS and CO<sub>2</sub> exhibited an  $r^2=0.61$ , likely

**Table 3.** Correlation coefficients, slopes, and standard errors of the linear correlation for each compound at each region. Regions denoted as reg1, reg2, and reg3 are shown in Fig. 1, and outside is the segment of the flight route excluding the three regions sampled by flight 13. SBL stands for the boundary layer over the southeastern US observed by flights 6, 7, 10, 12, 16, and 19. Ratios of O<sub>3</sub>-CO and CH<sub>4</sub>-CO are in unit of ppbv/ppbv, CO-CO<sub>2</sub> in ppbv/ppmv, CH<sub>4</sub>-CO<sub>2</sub> in ppmv/ppmv, COS-CO<sub>2</sub> in pptv/ppmv, and all others in pptv/ppbv.

|                                      | $r^2$ |      |       |         |      | Slope |       |         |         |        | Standard error of the slope |      |      |         |      |
|--------------------------------------|-------|------|-------|---------|------|-------|-------|---------|---------|--------|-----------------------------|------|------|---------|------|
|                                      | reg1  | reg2 | reg3  | outside | SBL  | Reg1  | reg2  | reg3    | outside | SBL    | reg1                        | reg2 | reg3 | outside | SBL  |
| O <sub>3</sub> -CO                   | 0.37  | 0.03 | 0.16  | 0.29    | 0.59 | 0.34  | 0.17  | -0.35   | 0.98    | 0.26   | 2.4                         | 0.84 | 1.6  | 0.35    | 0.03 |
| CH <sub>4</sub> -CO                  | 0.84  | 0.79 | 0.46  | 0.89    | 0.65 | 0.94  | 0.97  | 0.68    | 1.0     | 0.71   | 58                          | 22   | 45   | 11      | 0.17 |
| COS-CO                               | 0.42  | 0.45 | 0.42  | 0.59    | 0.41 | -0.45 | -0.77 | -0.83   | -0.59   | -0.73  | 14                          | 5.4  | 11   | 2.8     | 0.07 |
| CHCl <sub>3</sub> -CO                | 0.81  | 0.85 | 0.60  | 0.90    | 0.77 | 0.07  | 0.06  | 0.07    | 0.06    | 0.08   | 0.30                        | 0.11 | 0.23 | 0.06    | 0.01 |
| C <sub>2</sub> Cl <sub>4</sub> -CO   | 0.36  | 0.76 | 0.64  | 0.67    | 0.74 | 0.15  | 0.09  | 0.10    | 0.08    | 0.09   | 0.27                        | 0.06 | 0.15 | 0.02    | 0.01 |
| i-C <sub>5</sub> H <sub>12</sub> -CO | 0.38  | 0.53 | 0.79  | 0.40    | 0.17 | 0.19  | 0.23  | 0.36    | 0.14    | 0.82   | 0.19                        | 0.13 | 0.16 | 0.09    | 0.04 |
| C <sub>6</sub> H <sub>6</sub> -CO    | 0.22  | 0.66 | 0.73  | 0.55    | 0.57 | 0.13  | 0.31  | 0.29    | 0.25    | 0.64   | 0.24                        | 0.15 | 0.34 | 0.03    | 0.03 |
| C <sub>2</sub> H <sub>2</sub> -CO    | 0.89  | 0.77 | 0.76  | 0.84    | 0.87 | 1.5   | 1.7   | 1.5     | 1.5     | 2.6    | 2.8                         | 0.93 | 1.9  | 0.04    | 0.05 |
| CH <sub>4</sub> -CO <sub>2</sub>     | 0.08  | 0.71 | 0.002 | 0.86    | 0.46 | -0.01 | -0.01 | -0.0004 | -0.01   | -0.005 | 1.8                         | 0.28 | 0.48 | 0.11    | 0.04 |
| COS-CO <sub>2</sub>                  | 0.09  | 0.63 | 0.01  | 0.64    | 0.83 | 6.7   | 12    | 1.3     | 8.1     | 5.3    | 421                         | 69   | 117  | 1.8     | 0.37 |
| CO-CO <sub>2</sub>                   | 0.09  | 0.65 | 0.01  | 0.85    | 0.36 | -6.0  | -11   | -1.4    | -12     | -2.7   | 112                         | 17   | 30   | 0.81    | 0.2  |

driven to a large extent by their close association with vegetative uptake.

Correlations between source indicators and CO/CO<sub>2</sub> were examined further for each region and the results are presented in Table 3. The slope of CH<sub>4</sub>-CO had a value of 0.94 in region 1 ( $r^2=0.84$ ), 0.97 in region 2 ( $r^2=0.79$ ), and 0.68 in region 3 ( $r^2=0.46$ ). These values are reasonably close to the slope of 0.84 that was obtained for urban and industrial emissions by Harriss et al. (1994). To corroborate the urban and industrial influence, relationships between CO and a number of anthropogenic tracers were also examined. Compounds that correlated with CO at  $r^2>0.5$ , were CHCl<sub>3</sub> and C<sub>2</sub>H<sub>2</sub> in region 1, CHCl<sub>3</sub>, C<sub>2</sub>Cl<sub>4</sub>, i-C<sub>5</sub>H<sub>12</sub>, C<sub>6</sub>H<sub>6</sub>, and C<sub>2</sub>H<sub>2</sub> in region 2, and CHCl<sub>3</sub>, C<sub>2</sub>Cl<sub>4</sub>, i-C<sub>5</sub>H<sub>12</sub>, C<sub>6</sub>H<sub>6</sub> and C<sub>2</sub>H<sub>2</sub> in region 3. This evidence clearly points to a significant influence of urban, industrial, and combustion sources in all three regions.

To verify the SBL origin of the polluted air on flight 13, relationships between source indicators and CO in the SBL were calculated and the values of  $r^2$  and correlation slopes are shown in Table 3. The slopes of CHCl<sub>3</sub>-CO and C<sub>2</sub>Cl<sub>4</sub>-CO in the SBL were similar to those in the three flight regions, providing support for the SBL as the source region of the air masses encountered on the flight route. Note that slopes of i-C<sub>5</sub>H<sub>10</sub>-CO, C<sub>6</sub>H<sub>6</sub>-CO and C<sub>2</sub>H<sub>2</sub>-CO in the SBL were much higher than those observed on flight 13. For example, the slope of i-C<sub>5</sub>H<sub>10</sub>-CO in each region of flight 13 was between 0.19 and 0.36 compared to 0.82 in the SBL. The lifetimes of C<sub>2</sub>H<sub>2</sub>, C<sub>6</sub>H<sub>6</sub>, i-C<sub>5</sub>H<sub>12</sub>, C<sub>2</sub>Cl<sub>4</sub>, and CHCl<sub>3</sub> in the SBL were estimated to be 3.5, 2.4, 0.72, 17, and 29 days respectively. Therefore, maximum mixing ratios of short-lived i-C<sub>5</sub>H<sub>10</sub>, C<sub>6</sub>H<sub>6</sub>, and C<sub>2</sub>H<sub>2</sub> in the SBL were much higher than on flight 13 (Table 1), which resulted in higher slope values in the SBL.

It is curious that, contrary to the tight CH<sub>4</sub>-CO correlation observed on flight 13, CH<sub>4</sub> and CO data from city surveys in the Southeast exhibited a poor correlation ( $r^2=0.16$ ), although the slope of CH<sub>4</sub>-CO was 0.94, nearly identical to values observed in regions 1 and 2. The slope of CH<sub>4</sub>-CO in the SBL sampled by the DC-8 was 0.70, similar to region 3, but with much better correlation ( $r^2=0.73$ ) than the city surveys. The difference may be related to the multi-years of data collection for the city survey versus the flight 13 snapshot.

The slope of COS-CO<sub>2</sub> was compared between the SBL and over the North Atlantic. In the SBL CO<sub>2</sub> was correlated with COS at  $r^2=0.83$ , compared to  $r^2=0.61$  in the flight region. This difference is attributed to the mixing of SBL air with ambient air while it meandered over the Southeast for several days and then during transit to the upper troposphere. The COS-CO<sub>2</sub> slope value was 5.3 pptv/ppmv in the SBL, which was almost a factor of two lower than the 9.9 pptv/ppmv value obtained from the flight 13 regions. Mixing ratios of CO<sub>2</sub> in the SBL varied over the range 356 ppmv–380 ppmv, which was a factor of 5 wider than the range in the flight 13 region of 372 ppmv–377 ppmv. Similarly, the COS data showed the SBL had a factor of 2 greater variation in mixing ratios than the flight 13 data; 344 pptv–485 pptv in SBL and 411 pptv–479 pptv for the flight regions. Wider ranges of CO<sub>2</sub> and COS in the SBL are due to much lower minimum values of two compounds compared to the flight route. The higher minimum values along the flight path is indicative of a mixing process with the air mass types identified by our trajectory analysis. However, COS and CO<sub>2</sub> were not well correlated in regions 1 and 3, compared to region 2 and all the flight 13 data together.

A contribution of emissions from the Northeast to the flight regions was checked by utilizing UNH AIRMAP network data in New England. The  $r^2$  values and slopes of the correlations between selected trace gases and CO from ground-based measurements on 27–28 July (UTC) at TF (Thompson Farm) and AI (Appledore Island) were very different than those shown here for flight 13 (e.g., the slope of  $\text{CH}_4\text{--CO}=0.28$  ( $r^2=0.06$ ) at AI). Therefore, we concluded that emissions from the Northeast were not an important contributor to the elevated trace gas mixing ratios in the upper troposphere over the North Atlantic. This is consistent with our meteorological analysis which showed that the SBL was the likely primary source of pollutants in the upper troposphere.

An important feature of the flight 13 dataset was the high degree of correlation between trace gases in the Outside region. In fact, the correlations were close to, or better than, those in regions 1, 2, and 3 (e.g.,  $r^2=0.89$  for  $\text{CH}_4\text{--CO}$ ). This is a surprising result considering the diverse source regions indicated by our trajectory analysis. Typically, there is little or no correlation between most trace gases in air masses not directly impacted by relatively fresh continental emissions. In this case, it appears that the entire tropospheric column over the North Atlantic during the time period surrounding flight 13 was impacted by North American anthropogenic emissions. This region is in the direct outflow from the eastern US (Parrish et al., 1993), but our analysis seems to suggest that the troposphere over the mid-latitude North Atlantic basin was fumigated with US pollutants in various stages of aging. This is supported by the trajectory-based partitioning of the Outside air source regions, where 44% pointed to an influence of US continental outflow. Apparently, to retain their source relationships, these air masses were not mixed effectively with background marine air. The flight data demonstrate a pervasive impact of US anthropogenic emissions on the mid-latitude troposphere over the North Atlantic.

## 7 Summary

INTEX-NA, one of the components of ICARTT, was conducted over North America and the adjacent North Atlantic to investigate the distribution of trace gases and aerosols associated with emission sources in North America. The vertical distribution of trace gases from DC-8 flight 13 during the campaign had mixing ratios of  $\text{CH}_4$  and CO of up to 1843 ppbv and 134 ppbv respectively, and low mixing ratios of  $\text{CO}_2$  and COS, reduced to 372.4 ppmv and 411 pptv respectively, in upper troposphere at 8–11 km altitude over the North Atlantic.

The meteorology over the US was identified as an ideal situation for strong outflow for several days prior to flight 13. A stationary front, which evolved from a cold front associated with a Canadian low, existed in the eastern US over the sev-

eral days before the airborne measurements were conducted. As a result, it induced continuous convective activities and WCB uplifting of polluted air. In addition, a deep trough over the Midwest facilitated fast southwesterly transport that was sustained for several days prior to flight 13.

The chemical features in the upper troposphere over the North Atlantic were as follows. Urban and industrial tracers such as  $\text{CH}_4$  and CO were elevated in the upper troposphere (e.g. 78 ppbv < CO < 135 ppbv) and good linear relationships between the tracers (e.g.  $r^2$  for  $\text{CH}_4\text{--CO}$  at region 1=0.84) showed the impact of urban/industrial emissions to the flight regions. Low mixing ratios of COS and  $\text{CO}_2$  (e.g. 372.4 ppmv <  $\text{CO}_2$  < 376.6 ppmv) indicated biogenic uptake at the surface in the SBL with subsequent minimal dilution during the transport to the upper troposphere. Backward trajectories and photochemical aging indicated that the SBL was a potential source region for the chemical features. Agreement of the slopes for linear correlations of selected trace gases with a long atmospheric lifetime compared to the transport between SBL and flight regions support the SBL as the primary source region. Overall, meteorological and chemical analyses suggest rapid outflow from the SBL to the upper troposphere over the North Atlantic. In addition, the good linear correlation between urban and industrial tracers in whole flight regions ( $r^2$  for  $\text{CH}_4\text{--CO}=0.92$ ) and Outside ( $r^2$  for  $\text{CH}_4\text{--CO}=0.89$ ) suggest that the troposphere over the mid-latitude North Atlantic was influenced significantly with US pollutants in various stages of air mass processing.

*Acknowledgements.* This research benefited greatly from the combined effort of NASA DC-8 flight and science teams for INTEX-NA. We are grateful to the NASA Earth Science Tropospheric Chemistry Program for INTEX-NA funding which supported this work. Funding for this work was also provided by the NOAA AIRMAP grant #NA06OAR4600189, and fellowship support for SYK from the Climate Change Research Center at UNH. We also thank J.-P. Cammas and V. Thouret of the MOZAIC program, which is funded by the European Commission, CNRS (France), Forschungszentrum Jülich (Germany), Météo France, EADS (Airbus) and the airlines (Air France, Lufthansa, Austrian Airlines, and former Sabena who carry free of charge the MOZAIC equipment and perform the maintenance). Helpful discussions were provided by J. Hegarty and B. Sive.

Edited by: J. Williams

## References

- Arnold, S. R., Methven, J., Evans, M. J., et al.: Statistical inference of OH concentrations and air mass dilution rates from successive observations of nonmethane hydrocarbons in single air masses, *J. Geophys. Res.*, 112, D10S40, doi:10.1029/2006JD007594, 2007.
- Aucott, M. L., McCulloch, A., Graedel, T. E., Kleiman, G., Midgley, P., and Li, Y.-F.: Anthropogenic emissions



- of trichloromethane (chloroform,  $\text{CHCl}_3$ ) and chlorodifluoromethane (HCFC-22): Reactive Chlorine Emissions Inventory, *J. Geophys. Res.*, 104(D7), 8405–8415, 1999.
- Baker, A. K., Beyersdorf, A. J., Doezeema, L. A., Katzenstein, A., Meinardi, S., Simpson, I. J., Blake, D. R., and Rowland, F. S.: Measurements of Nonmethane Hydrocarbons in 28 United States Cities, *Atmos. Environ.*, 42, 170–182, 2008.
- Barletta, B., Meinardi, S., Simpson, I. J., Rowland, F. S., Chan, C.-Y., Wang, X., Zou, S., Chan, L. Y., and Blake, D. R.: Ambient halocarbon mixing ratios in 45 Chinese cities, *Atmos. Environ.*, 40, 7706–7719, 2006.
- Bartlett, K. B., Sachse, G. W., Collins Jr., J. E., and Harriss, R. C.: Methane in the tropical South Atlantic: Sources and distribution during the late dry season, *J. Geophys. Res.*, 101(D19), 24 139–24 150, 1996.
- Bartlett, K. B., Sachse, G. W., Slate, T., Harward, C., and Blake, D. R.: Large-scale distribution of  $\text{CH}_4$  in the western North Pacific: Sources and transport from the Asian continent, *J. Geophys. Res.*, 108(D20), 8807, doi:10.1029/2002JD003076, 2003.
- Blake, N. J., Blake, D. R., Simpson, I. J., et al.: NMHCs and halocarbons in Asian continental outflow during the Transport and Chemical Evolution over the Pacific (TRACE-P) Field Campaign: Comparison with PEM-West B., *J. Geophys. Res.*, 108(D20), 8806, doi:10.1029/2002JD003367, 2003.
- Brasseur, G. P., Orlando, J. J., and Tyndall, G. S.: *Atmospheric Chemistry and Global Change*, 654 pp., Oxford University Press, New York, 1999.
- Chan, L.-Y., Chu, K.-W., Zou, S.-C., Chan, C.-Y., Wang, X.-M., Barletta, B., Blake, D. R., Guo, H., and Tsai, W.-Y.: Characteristics of nonmethane hydrocarbons (NMHCs) in industrial, industrial-urban, and industrial-suburban atmospheres of the Pearl River Delta (PRD) region of south China, *J. Geophys. Res.*, 111, D11304, doi:10.1029/2005JD006481, 2006.
- Chin, M. and Davis, D. D.: Global sources and sinks of OCS and  $\text{CS}_2$  and their distributions, *Global Biogeochem. Cy.*, 7(2), 321–337, 1993.
- Colman, J. J., Swanson, A. L., Meinardi, S., Sive, B. C., Blake, D. R., and Rowland, F. S.: Description of the analysis of a wide range of volatile organic compounds in whole air samples collected during PEM-Tropics A and B, *Anal. Chem.*, 73, 3723–3731, 2001.
- Cooper, O. R., Moody, J. L., Parrish, D. D., Trainer, M., Ryerson, T. B., Holloway, J. S., Hübler, G., Fehsenfeld, F. C., Oltmans, S. J., and Evans, M. J.: Trace gas signatures of the airstreams within North Atlantic cyclones: Case studies from the North Atlantic Regional Experiment (NARE '97) aircraft intensive, *J. Geophys. Res.*, 106(D6), 5437–5456, 2001.
- Cooper, O. R., Stohl, A., Trainer, M., et al.: Large upper tropospheric ozone enhancements above midlatitude North America during summer: In situ evidence from the IONS and MOZAIC ozone measurement network, *J. Geophys. Res.*, 111, D24S05, doi:10.1029/2006JD007306, 2006.
- Crawford, J., Olson, J., Davis D., et al.: Clouds and trace gas distributions during TRACE-P, *J. Geophys. Res.*, 108(D21), 8818, doi:10.1029/2002JD003177, 2003.
- DeBell, L. J., Vozzella, M., Talbot, R. W., and Dibb, J. E.: Asian dust storm events of spring 2001 and associated pollutants observed in New England by the Atmospheric Investigation, Regional Modeling, Analysis and Prediction (AIRMAP) monitoring network, *J. Geophys. Res.*, 109, D01304, doi:10.1029/2003JD003733, 2004.
- Dickerson, R. R., Doddridge, B. G., Kelley, P., and Rhoads, K. P.: Large-scale pollution of the atmosphere over the remote Atlantic Ocean: Evidence from Bermuda, *J. Geophys. Res.*, 100(D5), 8945–8952, 1995.
- Fehsenfeld, F. C., Ancellet, G., Bates, T. S., et al.: International Consortium for Atmospheric Research on Transport and Transformation (ICARTT): North America to Europe – Overview of the 2004 summer field study, *J. Geophys. Res.*, 111, D23S01, doi:10.1029/2006JD007829, 2006.
- Fiore, A. M., Horowitz, L. W., Purves, D. W., Levy II, H., Evans, M. J., Wang, Y., Li, Q., and Yantosca, R. M.: Evaluating the contribution of changes in isoprene emissions to surface ozone trends over the eastern United States, *J. Geophys. Res.*, 110, D12303, doi:10.1029/2004JD005485, 2005.
- Fuelberg, H. E., Hannan, J. R., van Velthoven, P. F. J., Browell, E. V., Bieberbach Jr., G., Knabb, R. D., Gregory, G. L., Pickering, K. E., and Selkirk, H. B.: A meteorological overview of the Subsonic Assessment Ozone and Nitrogen Oxide Experiment (SONEX) period, *J. Geophys. Res.*, 105(D3), 3633–3651, 2000.
- Harriss, R. C., Sachse, G. W., Collins Jr., J. E., Wade, L., Bartlett, K. B., Talbot, R. W., Browell, E. V., Barrie, L. A., Hill, G. F., and Burney, L. G.: Carbon monoxide and methane over Canada: July–August 1990, *J. Geophys. Res.*, 99(D1), 1659–1669, 1994.
- Holton, J. R.: *An introduction to dynamic meteorology*, 511 pp., Academic Press, San Diego, 1992.
- Huntrieser, H., Heland, J., Schlager, H., et al.: Intercontinental air pollution transport from North America to Europe: Experimental evidence from airborne measurements and surface observations, *J. Geophys. Res.*, 110, D01305, doi:10.1029/2004JD005045, 2005.
- Jaffe, D., Anderson, T., Covert, D., Kotchenruther, R., Trost, B., Danielson, J., Simpson, W., Berntsen, T., Karlsdottir, S., Blake, D., Harris, J., Carmichael, G., and Uno, I.: Transport of Asian Air Pollution to North America, *Geophys. Res. Lett.*, 26(6), 711–714, 1999.
- Jaffe, D., McKendry, I., Anderson, T., and Price, H.: Six “new” episodes of trans-Pacific transport of air pollutants, *Atmos. Environ.*, 37, 391–404, 2003.
- Kiley, C. M. and Fuelbert, H. E.: An examination of summertime cyclone transport processes during Intercontinental Chemical Transport Experiment (INTEX-A), *J. Geophys. Res.*, 111, D24S06, doi:10.1029/2006JD007115, 2006.
- Lewis, A. C., Evans, M. J., Methven, J., et al.: Chemical composition observed over the mid-Atlantic and the detection of pollution signatures far from source regions, *J. Geophys. Res.*, 112, D10S39, doi:10.1029/2006JD007584, 2007.
- Li, Q., Jacob, D. J., Park, R., Wang, Y., Heald, C. L., Hudman, R., Yantosca, R. M., Martin, R. V., and Evans, M.: North American pollution outflow and the trapping of convectively lifted pollution by upper-level anticyclone, *J. Geophys. Res.*, 110, D10301, doi:10.1029/2004JD005039, 2005.
- Liang, Q., Jaeglé, L., Hudman, R. C., et al.: Summertime influence of Asian pollution in the free troposphere over North America, *J. Geophys. Res.*, 112, D12S11, doi:10.1029/2006JD007919, 2007.
- Mak, J. E. and Southon, J. R.: Assessment of tropical OH seasonality using atmospheric  $^{14}\text{CO}$  measurements from Barbados, *Geophys. Res. Lett.*, 35, L18301, doi:10.1029/2007GL031111, 2008.

- phys. Res. Lett., 25(15), 2801–2804, 1998.
- Mao, H., Talbot, R., Troop, D., Johnson, R., Businger, S., and Thompson, A. M.: Smart Balloon observations over the North Atlantic: O<sub>3</sub> data analysis and modeling, *J. Geophys. Res.*, 111, D23S56, doi:10.1029/2005JD006507, 2006.
- McKeen, S. A. and Liu, S. C.: Hydrocarbon ratios and photochemical history of air masses, *Geophys. Res. Lett.*, 20(21), 2363–2366, 1993.
- McKendry, I. G., Strawbridge, K. B., O'Neill, N. T., Macdonald, A. M., Liu, P. S. K., Leaith, W. R., Anlauf, K. G., Jaegle, L., Fairlie, T. D., and Westphal, D. L.: Trans-Pacific transport of Saharan dust to western North America: A case study, *J. Geophys. Res.*, 112, D01103, doi:10.1029/2006JD007129, 2007.
- Methven, J., Arnold, S. R., Stohl, A., et al.: Establishing Lagrangian connections between observations within air masses crossing the Atlantic during the International Consortium for Atmospheric Research on Transport and Transformation experiment, *J. Geophys. Res.*, 111, D23S62, doi:10.1029/2006JD007540, 2006.
- Millet, D. B., Goldstein, A. H., Holzinger, R., et al.: Chemical characteristics of North American surface layer outflow: Insights from Chebogue Point, Nova Scotia, *J. Geophys. Res.*, 111, D23S53, doi:10.1029/2006JD007287, 2006.
- Montzka, S. A., Calvert, P., Hall, B. D., Elkins, J. W., Conway, T. J., Tans, P. P., and Sweeney, C.: On the global distribution, seasonality, and budget of atmospheric carbonyl sulfide (COS) and some similarities to CO<sub>2</sub>, *J. Geophys. Res.*, 112, D09302, doi:10.1029/2006JD007665, 2007.
- Na, K., Kim, Y. P., Moon, K.-C., Moon, I., and Fung, K.: Concentrations of volatile organic compounds in an industrial area of Korea, *Atmos. Environ.*, 35, 2747–2756, 2001.
- Parrish, D. D., Holloway, J. S., Trainer, M., Murphy, P. C., Forbes, G. L., and Fehsenfeld, F. C.: Export of North American Ozone Pollution to the North Atlantic Ocean, *Science*, 259(5100), 1436–1439, 1993.
- Parrish, D. D., Dunlea, E. J., Atlas, E. L., et al.: Changes in the photochemical environment of the temperate North Pacific troposphere in response to increased Asian emissions, *J. Geophys. Res.*, 109, D23S18, doi:10.1029/2004JD004978, 2004.
- Pickering, K. E., Thompson, A. M., Wang, Y., Tao, W.-K., McNamara, D. P., Kirchhoff, V. W. J. H., Heikes, B. G., Sachse, G. W., Bradshaw, J. D., Gregory, G. L., and Blake, D. R.: Convective transport of biomass burning emissions over Brazil during TRACE A, *J. Geophys. Res.*, 101(D19), 23 993–24 012, 1996.
- Purvis, R. M., Lewis, A. C., Carney, R. A., et al.: Rapid uplift of nonmethane hydrocarbons in a cold front over central Europe, *J. Geophys. Res.*, 108(D7), 4224, doi:10.1029/2002JD002521, 2003.
- Reeves, C. E., Slemr, J., Oram, D. E., et al.: Alkyl nitrates in outflow from North America over the North Atlantic during Intercontinental Transport of Ozone and Precursors 2004, *J. Geophys. Res.*, 112, D10S27, doi:10.1029/2006JD007567, 2007.
- Sander, S. P., Finlayson-Pitts, B. J., Friedl, R. R., Golden, D. M., Huie, R. E., Kolb, C. E., Kurylo, M. J., Molina, M. J., Moortgat, G. K., Orkin, V. L., and Ravishankara, A. R.: Chemical Kinetics and Photochemical Data for Use in Atmospheric Studies, Evaluation Number 14, JPL Publication 02–25, Jet Propulsion Laboratory, Pasadena, CA., 2003.
- Sandoval-Soto, L., Stanimirov, M., von Hobe, M., Schmitt, V., Valdes, J., Wild, A., and Kesselmeier, J.: Global uptake of carbonyl sulfide (COS) by terrestrial vegetation: Estimates corrected by deposition velocities normalized to the uptake of carbon dioxide (CO<sub>2</sub>), *Biogeosciences*, 2, 125–132, 2005, <http://www.biogeosciences.net/2/125/2005/>.
- Simmonds, P. G., Manning, A. J., Cunnold, D. M., et al.: Global trends, seasonal cycles, and European emissions of dichloromethane, trichloroethene, and tetrachloroethene from the AGAGE observations at Mace Head, Ireland, and Cape Grim, Tasmania, *J. Geophys. Res.*, 111, D18304, doi:10.1029/2006JD007082, 2006.
- Singh, H. B., Brune, W. H., Crawford, J. H., Jacob, D. J., and Russell, P. B.: Overview of the summer 2004 Intercontinental Chemical Transport Experiment – North America (INTEX-A), *J. Geophys. Res.*, 111, D24S01, doi:10.1029/2006JD007905, 2006.
- Sive, B. C., Zhou, Y., Troop, D., Wang, Y., Little, W. C., Wingerter, O. W., Russo, R. S., Varner, R. K., and Talbot, R.: Development of a cryogen-free concentration system for measurements of volatile organic compounds, *Anal. Chem.*, 77(21), 6989–6998, doi:10.1021/ac0506231, 2005.
- Snow, J. A., Heikes, B. G., Shen, H., O'Sullivan, D. W., Fried, A., and Walega, J.: Hydrogen peroxide, methyl hydroperoxide, and formaldehyde over North America and the North Atlantic, *J. Geophys. Res.*, 112, D12S07, doi:10.1029/2006JD007746, 2007.
- Stohl, A., Forster, C., Eckhardt, S., Spichtinger, N., Huntrieser, H., Heland, J., Schlager, H., Wilhelm, S., Arnold, F., and Cooper, O.: A backward modeling study of intercontinental pollution transport using aircraft measurements, *J. Geophys. Res.*, 108(D12), 4370, doi:10.1029/2002JD002862, 2003.
- Talbot, R. W., Dibb, J. E., Klemm, K. I., Bradshaw, J. D., Sandholm, S. T., Blake, D. R., Sachse, G. W., Collins, J., Heikes, B. G., Gregory, G. L., Anderson, B. E., Singh, H. B., Thornton, D. C., and Merrill, J. T.: Chemical characteristics of continental outflow from Asia to the troposphere over the western Pacific Ocean during September–October 1991: Results from PEM-West A, *J. Geophys. Res.*, 101(D1), 1713–1725, 1996a.
- Talbot, R. W., Bradshaw, J. D., Sandholm, S. T., Smyth, S., Blake, D. R., Blake, N. R., Sachse, G. W., Collins, J. E., Heikes, B. G., Anderson, B. E., Gregory, G. L., Singh, H. B., Lefer, B. L., and Bachmeier, A. S.: Chemical characteristics of continental outflow over the tropical South Atlantic Ocean from Brazil and Africa, *J. Geophys. Res.*, 101(D19), 24 187–24 202, 1996b.
- Talbot, R. W., Dibb, J. E., Lefer, B. L., Bradshaw, J. D., Sandholm, S. T., Blake, D. R., Blake, N. J., Sachse, G. W., Collins Jr., J. E., Heikes, B. G., Merrill, J. T., Gregory, G. L., Anderson, B. E., Singh, H. B., Thornton, D. C., Bandy, A. R., and Poeschel, R. F.: Chemical characteristics of continental outflow from Asia to the troposphere over the western Pacific Ocean during February – March 1994: Results from PEM-West B, *J. Geophys. Res.*, 102(D23), 28 255–28 274, 1997.
- Twohy, C. H., Clement, C. F., Gandrud, B. W., et al.: Deep convection as a source of new particles in the midlatitude upper troposphere. *J. Geophys. Res.*, 107(D21), 4560, doi:10.1029/2001JD000323, 2002.
- Vay, S. A., Anderson, B. E., Conway, T. J., Sachse, G. W., Collins Jr., J. E., Blake, D. R., and Westberg, D. J.: Airborne observations of the tropospheric CO<sub>2</sub> distribution and its controlling factors over the South Pacific Basin, *J. Geophys. Res.*, 104(D5), 5663–5676, 1999.

- Wang, C. J.-L., Blake, D. R., and Rowland, F. S.: Seasonal variations in the atmospheric distribution of a reactive chlorine compound, tetrachloroethene ( $\text{CCl}_2=\text{CCl}_2$ ), *Geophys. Res. Lett.*, 22(9), 1097–1100, 1995.
- Wang, Y., Liu, S. C., Anderson, B. E., Kondo, Y., Gregory, G. L., Sachse, G. W., Vay, S. A., Blake, D. R., Singh, H. B., and Thompson, A. M.: Evidence of convection as a major source of condensation nuclei in the northern midlatitude upper troposphere, *Geophys. Res. Lett.*, 27(3), 369–372, 2000.
- Xiao, Y., Jacob, D. J., Wang, J. S., Logan, J. A., Palmer, P. I., Suntharalingam, P., Yantosca, R. M., Sachse, G. W., Blake, D. R., and Streets, D. G.: Constraints on Asian and European sources of methane from  $\text{CH}_4$ - $\text{C}_2\text{H}_6$ -CO correlations in Asian outflow, *J. Geophys. Res.*, 109, D15S16, doi:10.1029/2003JD004475, 2004.
- Zhou, Y., Varner, R. K., Russo, R. S., Wingenter, O. W., Haase, K. B., Talbot, R. W., and Sive, B. C.: Coastal water source of short-lived halocarbons in New England, *J. Geophys. Res.*, 110, D21302, doi:10.1029/2004JD005603, 2005.